

The responses to the comments of the Associate Editor in our direct reply (shown below) and within the revised manuscript (see marked copy) are provided. The pages and lines indicated below correspond to those in the marked copy.

### **Response to Associate Editor (Associate Editor's comments are italicized)**

1. Associate editor's comment: *"I partly agree with the anonymous reviewer #1 that the authors should add some discussions on the advantages and disadvantages of SF<sub>6</sub><sup>-</sup> chemistry compared to other ion chemistries that many people use (e.g. Iodide). Although some discussions are shown in the response to reviewers' comments, they are not available yet in the main text. I would encourage the authors to add 1-2 paragraphs either in or before Conclusions for this purpose, even though quantitative comparison may not be possible."*

**Author response:** As requested, we have added a couple of paragraphs into the revised manuscript pointing out the advantages and disadvantages (specifically, the sensitivities of organic acids) that SF<sub>6</sub><sup>-</sup>-CIMS has over I<sup>-</sup>-CIMS:

**Page 13 line 364:** "Nevertheless, these sensitivities are compared to formic and acetic acid sensitivities measured by a high-resolution time-of-flight chemical ionization mass spectrometer (Aerodyne Research Inc.) that utilized I<sup>-</sup> reagent ions during the field study. Only the formic and acetic acid sensitivities were compared since laboratory calibrations were not performed to determine the sensitivities for oxalic, butyric, glycolic, propionic and valeric acids by I<sup>-</sup>-CIMS. Although the formic acid sensitivity measured by I<sup>-</sup>-CIMS ( $1.33 \pm 0.28$  Hz ppt<sup>-1</sup>) was comparable to that measured by SF<sub>6</sub><sup>-</sup>-CIMS, the acetic acid sensitivity measured by I<sup>-</sup>-CIMS ( $< 0.1$  Hz ppt<sup>-1</sup>) was substantially lower than that measured by SF<sub>6</sub><sup>-</sup>-CIMS. Previous studies have similarly reported low acetic acid sensitivity measured by I<sup>-</sup>-CIMS (Aljawhary et al., 2013; Lee et al., 2014).

Since many recent studies use I<sup>-</sup> as a reagent ion to measure many compounds, the measured SF<sub>6</sub><sup>-</sup> sensitivities to organic acids are compared with those of I<sup>-</sup> reported by Lee et al. (2014, 2018). However, it is important to note that the absolute SF<sub>6</sub><sup>-</sup> and I<sup>-</sup> sensitivities values are specific to the respective instruments and their configuration. The sensitivity to individual compounds depend on a variety of instrument parameters (e.g., flow rates, pressures, electric fields, ion source activity) that control ion production and transmission, reaction time, declustering efficiency, etc. Consequently, this analysis serves primarily as a qualitative comparison of SF<sub>6</sub><sup>-</sup> and I<sup>-</sup> sensitivity.

Although the I<sup>-</sup> sensitivity to formic acid (2.9 Hz ppt<sup>-1</sup>) reported by Lee et al. (2014) is higher than that of SF<sub>6</sub><sup>-</sup> (1.29 Hz ppt<sup>-1</sup>), the SF<sub>6</sub><sup>-</sup> sensitivities for the other organic acids (i.e., acetic, oxalic, glycolic and propionic acids) are substantially higher than those of I<sup>-</sup> (Table S1a). The SF<sub>6</sub><sup>-</sup> CIMS method is particularly sensitive to oxalic, propionic and glycolic acids, which are expected to be present at low concentrations in the atmosphere. The sensitivities of SF<sub>6</sub><sup>-</sup> and I<sup>-</sup> to SO<sub>2</sub>, HNO<sub>3</sub> and HCl can also be compared (Table S1b). The SF<sub>6</sub><sup>-</sup> sensitivities of SO<sub>2</sub> and HCl are significantly higher than that of I<sup>-</sup> reported by Lee et al. (2018). However, I<sup>-</sup> is more sensitive to HNO<sub>3</sub>."

**Table S1a: Comparison of SF<sub>6</sub><sup>-</sup> vs. I<sup>-</sup> sensitivities of organic acids**

Organic Acid	I <sup>-</sup> sensitivity (Hz ppt <sup>-1</sup> ) <sup>a</sup>	SF <sub>6</sub> <sup>-</sup> sensitivity (Hz ppt <sup>-1</sup> )	
		X <sup>-</sup>	X <sup>-</sup> •HF
Formic acid	2.9	1.29 ± 0.22	0.29 ± 0.05
Acetic acid	0.1	1.46 ± 0.29	0.30 ± 0.06
Oxalic acid	0.21	6.38 ± 0.32	0.97 ± 0.05
Butyric acid	Not available	0.41 ± 0.01	0.12 ± 0.004
Glycolic acid	1.1	5.53 ± 0.11	1.64 ± 0.03
Propionic acid	0.066	2.05 ± 0.02	1.26 ± 0.01
Valeric acid	Not available	0.76 ± 0.008	0.35 ± 0.004

<sup>a</sup>The I<sup>-</sup> sensitivities shown here are those reported by Lee et al. (2014). The organic acids were detected as cluster ions with iodide (I(X)<sup>-</sup>).

**Table S1b: Comparison of SF<sub>6</sub><sup>-</sup> vs. I<sup>-</sup> sensitivities of inorganic compounds**

Inorganic compound	I <sup>-</sup> sensitivity (Hz ppt <sup>-1</sup> ) <sup>b</sup>	SF <sub>6</sub> <sup>-</sup> sensitivity (Hz ppt <sup>-1</sup> )
SO <sub>2</sub>	0.028	2.9
HNO <sub>3</sub>	9.0	5.8 for NO <sub>3</sub> <sup>-</sup> , 0.2 for NO <sub>3</sub> <sup>-</sup> •HF <sup>c</sup>
HCl	0.03	1.4 <sup>d</sup>

<sup>b</sup>The I<sup>-</sup> sensitivities shown here are those reported by Lee et al. (2018).

<sup>c</sup>The high collision energy used in the CDC promoted the dissociation of NO<sub>3</sub><sup>-</sup>•HF ions, causing the low sensitivity at NO<sub>3</sub><sup>-</sup>•HF.

<sup>d</sup>HCl was detected as SF<sub>5</sub>Cl<sup>-</sup>.

## References:

Aljawhary, D., Lee, A. K. Y., and Abbatt, J. P. D.: High-resolution chemical ionization mass spectrometry (ToF-CIMS): application to study SOA composition and processing, *Atmospheric Measurement Techniques*, 6, 3211-3224, 10.5194/amt-6-3211-2013, 2013.

Lee, B. H., Lopez-Hilfiker, F. D., Mohr, C., Kurten, T., Worsnop, D. R., and Thornton, J. A.: An Iodide-Adduct High-Resolution Time-of-Flight Chemical-Ionization Mass Spectrometer: Application to Atmospheric Inorganic and Organic Compounds, *Environmental Science & Technology*, 48, 6309-6317, 10.1021/es500362a, 2014.

Lee, B. H., Lopez-Hilfiker, F. D., Veres, P. R., McDuffie, E. E., Fibiger, D. L., Sparks, T. L., Ebben, C. J., Green, J. R., Schroder, J. C., Campuzano-Jost, P., Iyer, S., D'Ambro, E. L., Schobesberger, S., Brown, S. S., Wooldridge, P. J., Cohen, R. C., Fiddler, M. N., Bililign, S., Jimenez, J. L., Kurtén, T., Weinheimer, A. J., Jaegle, L., and Thornton, J. A.: Flight Deployment of a High-Resolution Time-of-Flight Chemical Ionization Mass Spectrometer: Observations of Reactive Halogen and Nitrogen Oxide Species, *Journal of Geophysical Research: Atmospheres*, 0, doi:10.1029/2017JD028082, 2018.

2. Associate editor's comment: *"It should be noted that detection of SO<sub>2</sub> using I<sup>-</sup> chemistry was recently demonstrated (Lee et al., 2018). As a result, the sentence "the major advantage that SF<sub>6</sub><sup>-</sup> has over I<sup>-</sup> and CH<sub>3</sub>CO<sub>2</sub><sup>-</sup> is that it allows for the detection of acetic acid and SO<sub>2</sub>". (L110-L111) is not totally accurate. Detection of acetic acid is also possible using I<sup>-</sup>, but not ideal, as shown in Lee et al., 2014."*

**Author response:** We agree that the Associate Editor has a good point. Lee et al. (2018) did measure SO<sub>2</sub> in a nocturnal power plant plume using the I<sup>-</sup> reagent ion with a high-resolution TOF mass spectrometer, but they also showed that the sensitivity was approximately 100 times lower than that for formic acid. Hence, we have cited this paper and have revised the manuscript as follows:

**Page 4 line 110: "The major advantage that SF<sub>6</sub><sup>-</sup> has over I<sup>-</sup> and CH<sub>3</sub>CO<sub>2</sub><sup>-</sup> in this study is that it offers the possibility of sensitive detection of acetic and oxalic acids and SO<sub>2</sub> (Lee et al., 2014; Lee et al., 2018)."**

#### **References:**

**Lee, B. H., Lopez-Hilfiker, F. D., Mohr, C., Kurten, T., Worsnop, D. R., and Thornton, J. A.: An Iodide-Adduct High-Resolution Time-of-Flight Chemical-Ionization Mass Spectrometer: Application to Atmospheric Inorganic and Organic Compounds, Environmental Science & Technology, 48, 6309-6317, 10.1021/es500362a, 2014.**

**Lee, B. H., Lopez-Hilfiker, F. D., Veres, P. R., McDuffie, E. E., Fibiger, D. L., Sparks, T. L., Ebben, C. J., Green, J. R., Schroder, J. C., Campuzano-Jost, P., Iyer, S., D'Ambro, E. L., Schobesberger, S., Brown, S. S., Wooldridge, P. J., Cohen, R. C., Fiddler, M. N., Bililign, S., Jimenez, J. L., Kurtén, T., Weinheimer, A. J., Jaegle, L., and Thornton, J. A.: Flight Deployment of a High-Resolution Time-of-Flight Chemical Ionization Mass Spectrometer: Observations of Reactive Halogen and Nitrogen Oxide Species, Journal of Geophysical Research: Atmospheres, 0, doi:10.1029/2017JD028082, 2018.**

1 **Real-time measurements of gas-phase organic acids using SF<sub>6</sub><sup>-</sup> chemical ionization**  
2 **mass spectrometry**

3  
4 Theodora Nah,<sup>1,a</sup> Yi Ji,<sup>1,2</sup> David J. Tanner,<sup>1</sup> Hongyu Guo,<sup>1</sup> Amy P. Sullivan,<sup>3</sup> Nga Lee  
5 Ng,<sup>1,2</sup> Rodney J. Weber<sup>1</sup> and L. Gregory Huey<sup>1\*</sup>  
6

7 <sup>1</sup>*School of Earth and Atmospheric Sciences, Georgia Institute of Technology, Atlanta, GA, USA*

8 <sup>2</sup>*School of Chemical and Biomolecular Engineering, Georgia Institute of Technology, Atlanta, GA, USA*

9 <sup>3</sup>*Department of Atmospheric Science, Colorado State University, Fort Collins, CO, USA*

10 <sup>a</sup>*Now at School of Energy and Environment, City University of Hong Kong, Kowloon, Hong Kong, China*

11 *\* To whom correspondence should be addressed: greg.huey@eas.gatech.edu*  
12

13 **Abstract**

14 The sources and atmospheric chemistry of gas-phase organic acids are currently poorly  
15 understood due in part to the limited range of measurement techniques available. In this  
16 work, we evaluated the use of SF<sub>6</sub><sup>-</sup> as a sensitive and selective chemical ionization reagent  
17 ion for real-time measurements of gas-phase organic acids. Field measurements are made  
18 using a chemical ionization mass spectrometer (CIMS) at a rural site in Yorkville, Georgia  
19 from September to October 2016 to investigate the capability of this measurement  
20 technique. Our measurements demonstrate that SF<sub>6</sub><sup>-</sup> can be used to measure a range of  
21 organic acids in the atmosphere. 1-hour averaged ambient concentrations of organic acids  
22 ranged from a few parts per trillion by volume (ppt) to several parts per billion by volume  
23 (ppb). All the organic acids displayed similar strong diurnal behaviors, reaching maximum  
24 concentrations between 5 and 7 pm local time. The organic acid concentrations are  
25 dependent on ambient temperature, with higher organic acid concentrations being  
26 measured during warmer periods.

27 **Introduction**

28 Organic acids are ubiquitous and important species in the troposphere. They are  
29 major contributors of free acidity in precipitation (Galloway et al., 1982; Keene et al., 1983;  
30 Keene and Galloway, 1984), and can also affect the formation of secondary organic  
31 aerosols (SOA) (Zhang et al., 2004; Carlton et al., 2006; Sorooshian et al., 2010; Yatavelli  
32 et al., 2015). As end products of oxidation, organic acids can also serve as useful tracers of  
33 air mass history (Sorooshian et al., 2007; Sorooshian et al., 2010). Organic acids are found  
34 in urban, rural and remote marine environments in the gas, aqueous and particle phases.

35 While organic acids are emitted directly from biogenic sources (e.g., microbial activity,  
36 vegetation and soil) and anthropogenic activities (e.g., fossil fuel combustion, vehicular  
37 emissions and biomass burning) (Kawamura et al., 1985; Talbot et al., 1988; Chebbi and  
38 Carlier, 1996; Talbot et al., 1999; Seco et al., 2007; Veres et al., 2010; Paulot et al., 2011;  
39 Veres et al., 2011; Millet et al., 2015), they can also be formed from photooxidation of  
40 non-methane volatile organic compounds and aqueous-phase photochemistry of semi-  
41 volatile organic compounds (Chebbi and Carlier, 1996; Hansen et al., 2003; Orzechowska  
42 and Paulson, 2005; Carlton et al., 2006; Sorooshian et al., 2007; Ervens et al., 2008; Paulot  
43 et al., 2011; Millet et al., 2015). The chemical aging of organic aerosols has also been  
44 proposed as a major source of organic acids (Molina et al., 2004; Vlasenko et al., 2008;  
45 Paulot et al., 2011). The relative importance of primary and secondary sources of organic  
46 acids are currently poorly constrained though their emissions likely depend on the  
47 magnitude of biogenic and anthropogenic activities and the meteorological conditions. Wet  
48 and dry deposition are the primary sinks of organic acids in the atmosphere (Chebbi and  
49 Carlier, 1996).

50 Formic and acetic acids are the dominant gas-phase monocarboxylic acids in the  
51 troposphere (Chebbi and Carlier, 1996). Due to their high vapor pressures, the gas-phase  
52 concentrations of formic and acetic acids are usually 1 to 2 orders of magnitudes higher  
53 than their particle-phase concentrations. Some field studies report strong correlations  
54 between formic and acetic acids, suggesting that these two organic acids have similar  
55 sources (Nolte et al., 1997; Souza and Carvalho, 2001; Paulot et al., 2011). A recent  
56 modeling study suggested that the dominant sources of formic acid in the southeastern U.S.  
57 are primarily biogenic in nature (Millet et al., 2015). These sources include direct emissions  
58 from vegetation and soil and photochemical production from biogenic volatile organic  
59 compounds (BVOCs). Currently, atmospheric formic and acetic acid concentrations are  
60 higher than those predicted by models, indicating that present model estimates of source  
61 and sink magnitudes are incorrect (Paulot et al., 2011; Millet et al., 2015). In the case of  
62 formic acid, deposition and secondary photochemical production via mechanisms such as  
63 photooxidation of isoprene and reaction of stabilized criegee intermediates need to be  
64 better constrained in models. Given that formic and acetic acids are major trace gases in  
65 the atmosphere, there is a need to resolve the discrepancy between measurements and

66 model predictions to close the atmospheric reactive carbon budget and improve our overall  
67 understanding of VOC chemistry in the atmosphere.

68 Currently, research on gas-phase organic acids has focused primarily on formic and  
69 acetic acids (Andreae et al., 1988; Talbot et al., 1988; Grosjean, 1991; Hartmann et al.,  
70 1991; Talbot et al., 1995; Talbot et al., 1999). This is due, in part, to the analytical  
71 difficulties in measuring gas-phase  $> C_2$  organic acids and oxidized organic acids (i.e.,  
72 containing more than 2 oxygen atoms) in real time. These organic acids have low vapor  
73 pressures and are generally present in low concentrations in the gas phase. For example,  
74 dicarboxylic acids typically have vapor pressures that are 2 to 4 orders of magnitude lower  
75 than their analogous monocarboxylic acids (Chebbi and Carlier, 1996), and are present  
76 mainly in the particle and aqueous phases. Rapid and accurate measurements of gas-phase  
77  $> C_2$  organic acids and oxidized organic acids are necessary for constraining the regional  
78 and global SOA budget since these acids can partition readily between the gas and particle  
79 and aqueous phases and subsequently affect SOA formation (Zhang et al., 2004; Carlton  
80 et al., 2006; Ervens et al., 2008; Sorooshian et al., 2010; Yatavelli et al., 2015).

81 Chemical ionization mass spectrometry (CIMS) is commonly used to selectively  
82 measure atmospheric trace gases in real-time with high sensitivity. CIMS measurements  
83 rely on reactions between reagent ions and compounds of interest present in the sampled  
84 air to produce analyte ions that are detected by a mass spectrometer. The subset of  
85 molecular species detected is determined by the reagent ion employed since the specificity  
86 of the ionization process is governed by the ion-molecule reaction mechanism. CIMS is a  
87 popular tool for atmospheric measurements since it is versatile and has high time resolution  
88 and sensitivity. It is also often a soft ionization technique with minimal ion fragmentation,  
89 thus preserving the parent molecule's elemental composition and allowing for molecular  
90 speciation. Recent developments in chemical ionization methods and sources have greatly  
91 improved our ability to measure atmospheric acidic species. Some of the CIMS reagent  
92 ions that have been used to measure atmospheric organic acids include acetate ( $CH_3CO_2^-$ ),  
93 iodide ( $I^-$ ) and  $CF_3O^-$  anions (Crounse et al., 2006; Veres et al., 2008; Lee et al., 2014;  
94 Brophy and Farmer, 2015; Nguyen et al., 2015). However, each of these CIMS reagent  
95 ions has its drawbacks, which are generally related to their selectivity and sensitivity

96 towards different atmospheric species. For example, acetic acid is difficult to measure with  
97  $\text{CH}_3\text{CO}_2^-$  as the CIMS reagent ion due to interferences from the reagent ion chemistry that  
98 complicates the desired ion-molecule reactions. In addition, while many organic acids can  
99 be detected using  $\text{I}^-$  as a reagent ion, its sensitivity to different acids can vary by orders of  
100 magnitude (Lee et al., 2014).

101 The sulfur hexafluoride ( $\text{SF}_6^-$ ) anion has been used as a CIMS reagent ion to  
102 measure atmospheric inorganic species such as sulfur dioxide ( $\text{SO}_2$ ), nitric acid ( $\text{HNO}_3$ )  
103 and peroxyxynitric acid ( $\text{HO}_2\text{NO}_2$ ) (Slusher et al., 2001; Slusher et al., 2002; Huey et al.,  
104 2004; Kim et al., 2007).  $\text{SF}_6^-$  commonly reacts with most acidic gases at the collision rate  
105 by either proton or fluoride transfer reactions (Huey et al., 1995). The  $\text{SF}_6^-$  ion chemistry  
106 is selective to acidic species, which can simplify the mass spectral analysis of organic acids.  
107 However,  $\text{SF}_6^-$  is reactive to both ozone ( $\text{O}_3$ ) and water vapor, which can lead to interfering  
108 reactions that limit its applicability to many species in certain environments (Huey et al.,  
109 2004). For these reasons, this work is focused on assessing the ability of  $\text{SF}_6^-$  to measure a  
110 series of organic acids in ambient air. The major advantage that  $\text{SF}_6^-$  has over  $\text{I}^-$  and  
111  $\text{CH}_3\text{CO}_2^-$  [in this study](#) is that it [offers the possibility of sensitive](#) detection of acetic [and](#)  
112 [oxalic](#) acids and  $\text{SO}_2$  (Lee et al., 2014; Lee et al., 2018).  $\text{CF}_3\text{O}^-$  has a similar chemistry to  
113  $\text{SF}_6^-$  but it also has issues due to hydrolysis and the ion precursor is not commercially  
114 available. We present ambient measurements of gas-phase organic acids conducted in a  
115 mixed forest-agricultural area in Georgia in early fall of 2016 to evaluate the performance  
116 of a  $\text{SF}_6^-$  CIMS technique. Gas-phase organic acid measurements are compared to gas-  
117 phase water-soluble organic carbon ( $\text{WSOC}_g$ ) measurements performed during the field  
118 study to estimate the fraction of  $\text{WSOC}_g$  that is comprised of organic acids at this rural site.  
119 Laboratory experiments are conducted to measure the sensitivity of  $\text{SF}_6^-$  with a series of  
120 organic acids of atmospheric relevance.

## 121 2. Methods

### 122 2.1. Field site

123 Real-time ambient measurements of gas-phase organic acids were obtained using a  
124 chemical ionization mass spectrometer from 3 Sept to 12 Oct 2016 at the SouthEastern

Deleted: allows for the

126 Aerosol Research and Characterization (SEARCH) site located in Yorkville, Georgia. A  
127 detailed description of the field site has been provided by Hansen et al. (2003). Briefly, the  
128 Yorkville field site (33.931 N, 85.046 W) was located ~55 km northwest of Atlanta (the  
129 closest urban center), and was on a broad ridge in a large pasture where there were  
130 occasionally grazing cattle. The field site was surrounded by forest and agricultural land.  
131 There were no major roads near the field site and nearby traffic emissions were negligible.  
132 The closest power plant was Plant Bowen, which was located ~25 km north of the field  
133 site. The sampling period was characterized by moderate temperatures (24.0 °C average,  
134 32.6 °C max, 9.5 °C min) and high relative humidities (68.9 % RH average, 100 % RH  
135 max, 21.6 % RH min). The study-averaged diurnal trends of relative humidity, temperature  
136 and solar radiance are shown in Fig. S1. Data reported are displayed in EDT. Volumetric  
137 gas concentrations reported are at ambient temperature and relative humidity.

## 138 **2.2. SF<sub>6</sub>-CIMS**

### 139 **2.2.1. CIMS instrument and air sampling inlet**

140 The CIMS instrument was housed in a temperature-controlled trailer during the  
141 field study. The inlet configuration and CIMS instrument used in this study is shown in  
142 Fig. 1. Since HNO<sub>3</sub> and organic acids may condense on surfaces, an inlet configuration  
143 with a minimal wall interaction was used. This inlet configuration was previously described  
144 by Huey et al. (2004) and Nowak et al. (2006); hence, only a brief description will be  
145 provided here. The inlet was a 7.6 cm ID aluminum pipe that extended ~40 cm into the  
146 ambient air through a hole in the trailer's wall. This positioned the inlet ~2 m above the  
147 ground. A donut-shaped ring was attached to the ambient sampling port of the pipe to  
148 reduce the influence of crosswinds on the pipe's flow dynamics. This ring was wrapped  
149 with a fine wire mesh to prevent insects from being drawn through the pipe. A flow of  
150 ~2800 L min<sup>-1</sup> was maintained in the pipe using a regenerative blower (AMETEK  
151 Windjammer 116637-03). Part of this flow (7 L min<sup>-1</sup>) was sampled through a custom-  
152 made three-way PFA Teflon valve, which connected the pipe's center to the CIMS  
153 sampling orifice. The valve was maintained at a temperature of 40 °C in an insulated  
154 aluminum oven and could be switched automatically between ambient and background



155 modes. In ambient mode, ambient air was passed through a 25 cm long, 0.65 cm ID Teflon  
156 tube into the CIMS. In background mode, ambient air was first drawn through an activated  
157 charcoal scrubber before being delivered into the CIMS. A small flow of ambient air ( $\sim 0.05$   
158  $\text{L min}^{-1}$ ) was continuously passed through the scrubber to keep it at equilibrium with  
159 ambient humidity levels. Most of the sampled air flow ( $6.7 \text{ L min}^{-1}$ ) was exhausted using  
160 a small diaphragm pump. The rest of the sampled air flow ( $0.3 \text{ L min}^{-1}$ ) was introduced  
161 into the CIMS instrument through an automatic variable orifice, which was used to  
162 maintain a constant sample air mass flow.

163 The CIMS instrument was comprised of a series of differentially pumped regions:  
164 a flow tube, a collisional dissociation chamber, an octopole ion guide, a quadrupole mass  
165 filter and an ion detector. These sections were evacuated by a scroll pump (Edward nXDS  
166 20i), a drag pump (Adixen MDP 5011) and two turbo pumps (Varian Turbo-V301),  
167 respectively. Ambient air was drawn continuously into the flow tube. A flow of 3.7  
168 standard liter per minute (slpm) of  $\text{N}_2$  containing a few ppm of  $\text{SF}_6$  (Scott-Marrin Inc.) was  
169 passed through a  $^{210}\text{Po}$  ion source into the flow tube.  $\text{SF}_6^-$  anions, which were produced via  
170 associative electron attachment in the  $^{210}\text{Po}$  ion source, reacted with the sampled ambient  
171 air in the flow tube to generate analyte ions. Arnold and Viggiano (2001) showed that the  
172 formation of  $\text{F}\cdot(\text{HF})_n$  cluster ions from the reaction of  $\text{SF}_6^-$  and water vapor is enhanced at  
173 high flow tube pressures. Since these  $\text{F}\cdot(\text{HF})_n$  cluster ions could interfere with mass  
174 spectral analysis, the flow tube was maintained at a low pressure ( $\sim 13 \text{ mbar}$ , 0.5 %  
175 uncertainty) in this study to reduce both the water vapor concentration and reaction time in  
176 the flow tube, thus minimizing interferences from  $\text{SF}_6^-$  reaction with water vapor. The  
177 analyte ions exited the flow tube and were accelerated through the collisional dissociation  
178 chamber (CDC), which was maintained at  $\sim 0.8 \text{ mbar}$  (10 % uncertainty). The molecular  
179 collisions in the CDC served to dissociate weakly bound cluster ions into their core ions to  
180 simplify mass spectral analysis. Flow tube and CDC pressures were controlled by the  
181 automatic variable orifice. For this study, the CDC was operated at a relatively high electric  
182 field ( $\sim 113 \text{ V cm}^{-1}$ ) to efficiently dissociate cluster ions. The resulting ions were then  
183 passed into the octopole ion guide (maintained at  $\sim 6 \times 10^{-3} \text{ mbar}$ ), which collimated the  
184 ions and transferred them into the quadrupole mass spectrometer (maintained at  $\sim 10^{-5}$   
185 mbar) for mass selection and detection. It should also be noted that we always used gloves

186 when working on the CIMS during this study to limit contamination of lactic acid  
187 emissions from human skin. In addition, we kept people away from the front of the SF<sub>6</sub>-  
188 CIMS sampling inlet to minimize lactic acid interferences as well.

189 Ions monitored during the field study included mass-to-charge ratio (m/z) 45, 59,  
190 65, 73, 75, 79, 82, 87, 89, 101, 102, 103, 108, 117, 131 and 148. The assignment of these  
191 ions will be discussed in section 3. The dwell time for each m/z ion was set to 0.5 s and  
192 measurements of these ions were obtained every ~13 s, which resulted in a ~4 % (= 0.5/13  
193 x 100 %) duty cycle for each ion monitored. The data presented in this paper was averaged  
194 to 1-hour intervals unless stated otherwise.

### 195 **2.2.2. Background and calibration measurements during field study**

196 Background measurements were performed every 25 min during the field study.  
197 During each background measurement, the sampled air flow was passed through an  
198 activated charcoal scrubber prior to delivery into the CIMS. The scrubber removed > 99 %  
199 of the targeted species in ambient air. Calibration measurements were performed every 5 h  
200 during the field study through standard additions of <sup>34</sup>SO<sub>2</sub> and either formic or acetic acid  
201 to the sampled air flow. Each background and calibration measurement period lasted ~4  
202 and ~3.5 min, respectively, which not only gave the scrubber (during background  
203 measurements) and flow tube ample time to equilibrate when the three-way PFA Teflon  
204 valve was switched between ambient and background modes, but also allowed us to obtain  
205 good averaging statistics during background and calibration measurements. A 1.12 ppm  
206 <sup>34</sup>SO<sub>2</sub> gas standard was used as the source of the sulfur standard addition. 1.85 ppb of <sup>34</sup>SO<sub>2</sub>  
207 was added to sampled air flow during calibration measurements. The formic and acetic  
208 acid calibration sources were permeation tubes (VICI Metronics) with emission rates of 91  
209 and 110 ng min<sup>-1</sup>, respectively. The emission rates were measured by scrubbing the output  
210 of the permeation tube in deionized water via a gas impinger immersed in water, which  
211 was then analyzed for formate and acetate using ion chromatography (Thermo Fisher  
212 Scientific). Eight samples of each acid were analyzed over the course of the field study and  
213 the standard deviations of the permeation rates were ≤ 6 %. 6.75 ppb of formic acid and  
214 5.87 ppb of acetic acid was added to sampled air flow during calibration measurements.  
215 The CIMS instrument sensitivity measured by the F<sub>2</sub><sup>34</sup>SO<sub>2</sub><sup>-</sup> ion signal (m/z 104) was

216 similarly applied to all the other measured species (except for formic and acetic acids)  
217 using relative sensitivities determined in laboratory studies. The  $F_2^{34}SO_2^-$  calibrant ion  
218 signals were also used to calibrate ambient  $F_2^{32}SO_2^-$  ion signals and determine ambient  $SO_2$   
219 concentrations as discussed in section 3.2.5.

### 220 **2.2.3. Laboratory calibration**

221 To estimate the levels of sensitivities for a series of acids of atmospheric relevance,  
222  $HNO_3$ , oxalic, butyric, glycolic, propionic and valeric acid standard addition calibrations  
223 were performed in post-field laboratory work. Many of these acids have previously been  
224 measured in rural and urban environments (Kawamura et al., 1985; Veres et al., 2011;  
225 Brophy and Farmer, 2015). The response of the CIMS acid signals were measured relative  
226 to the sensitivity of  $^{34}SO_2$  in these calibration measurements. The  $HNO_3$  calibration source  
227 was a permeation tube (KIN-TEK) with a permeation rate of  $39 \text{ ng min}^{-1}$ , which was  
228 measured using UV optical absorption (Neuman et al., 2003). Solid or liquid samples of  
229 oxalic (Sigma Aldrich,  $\geq 99 \%$ ), butyric (Sigma Aldrich,  $\geq 99 \%$ ), glycolic (Sigma Aldrich,  
230  $99 \%$ ), propionic (Sigma Aldrich,  $\geq 99.5 \%$ ) and valeric (Sigma Aldrich,  $\geq 99 \%$ ) acids  
231 were used in calibration measurements. The acid sample was placed in a glass impinger,  
232 which was immersed in an ice bath to provide a constant vapor pressure. A flow of 6 to 10  
233  $\text{mL min}^{-1}$  of  $N_2$  was passed over the organic acid in the glass impinger. This organic acid  
234 air stream was then diluted with varying flows of  $N_2$  ( $1$  to  $5 \text{ L min}^{-1}$ ) to achieve different  
235 mixing ratios of the organic acid. Mixing ratios were calculated from either the acid's  
236 emission rate from the impinger or the acid's vapor pressure. The emission rate of gas-  
237 phase oxalic acid from the impinger was measured by scrubbing the output in deionized  
238 water using the same method for calibrating the formic and acetic acid permeation tubes,  
239 followed by ion chromatography analysis for oxalate. Three samples were analyzed and  
240 the emission rate was determined to be  $14 \text{ ng min}^{-1}$  with a standard deviation of  $< 5 \%$ . The  
241 vapor pressures of butyric and propionic acids at  $0 \text{ }^\circ\text{C}$  were measured using a capacitance  
242 manometer (MKS Instruments). The vapor pressures of glycolic and valeric acids at  $0 \text{ }^\circ\text{C}$   
243 were estimated using their literature vapor pressures at  $25 \text{ }^\circ\text{C}$  and enthalpies of vaporization  
244 (Daubert and Danner, 1989; Lide, 1995; Acree and Chickos, 2010).

245 Attempts to generate a calibration plot for pyruvic acid using its liquid sample  
246 (Sigma Aldrich, 98 %) and the setup described above were unsuccessful as this acid was  
247 found to interact very strongly with surfaces. Glyoxylic acid calibrations were not  
248 performed due to the presence of impurities in the glyoxylic acid monohydrate solution  
249 used (Sigma Aldrich, 98 %), which resulted in the appearance of ions not attributed to  
250 glyoxylic acid. We attempted to generate calibration plots for malonic (Sigma Aldrich,  $\geq$   
251 99.5 %), succinic (Sigma Aldrich, 99 %) and glutaric (Sigma Aldrich, 99 %) acids by  
252 passing N<sub>2</sub> over their solid samples at room temperature. However, it was not possible to  
253 generate large enough gas phase concentrations for calibration since these organic acids  
254 have very low vapor pressures. The vapor pressures of malonic, succinic and glutaric acids  
255 are  $5.73 \times 10^{-4}$ ,  $1.13 \times 10^{-4}$  and  $4.21 \times 10^{-4}$  kPa at 298 K, respectively (Booth et al., 2010),  
256 which are at least 2 orders of magnitude lower than the organic acids that we calibrated.  
257 Although heating up the malonic, succinic and glutaric acid samples will likely generate  
258 sufficient vapors for calibration, this method of generating calibrant gases will lead to large  
259 measurement uncertainties due to vapors condensing out and adhering onto surfaces at  
260 room temperature prior to introduction into the CIMS.

#### 261 **2.2.4. Detection limits and measurement uncertainties**

262 The detection limits of the organic acids were estimated as 3 times the standard  
263 deviation values ( $3\sigma$ ) of the ion signals measured during background mode. Although each  
264 background measurement period lasted  $\sim 4$  min, ion signals of the different organic acids  
265 took up to 1.5 min to stabilize during the switch between ambient, calibration and  
266 background measurements during the field study. Thus, ion signals measured during the  
267 first 1.5 min were not included in the calculation of the average and standard deviation of  
268 ion signals measured during background mode. Table 1 summarizes the average detection  
269 limits of calibrated organic acids for 2.5 min averaging periods which corresponds to the  
270 length of a background measurement with a 4 % duty cycle for each m/z. The mean  
271 difference between successive background measurements ranged from 1 to 40 ppt for the  
272 different organic acids. Future work will focus on reducing the instrument background, and  
273 therefore improving the detection limits of these organic acids.

274 The uncertainties ( $1\sigma$ ) in our ambient measurements of formic, acetic and oxalic  
275 acid concentrations originated from CIMS and ion chromatography calibration  
276 measurements. The ion chromatography measurement uncertainty was estimated to be 10  
277 %. For formic and acetic acids, which were calibrated during the field study using  
278 permeation tubes, their CIMS measurement uncertainties were estimated to be 6 and 7 %,  
279 respectively, based on one standard deviation of the acids' calibrant ion signals. For oxalic  
280 acid, which was calibrated in post-field laboratory work, the CIMS measurement  
281 uncertainty was estimated to be 9 % based on one standard deviation of the  $^{34}\text{SO}_2$   
282 sensitivity (3 %), the acid's calibrant ion signals (7 %) and linear fit of the calibration curve  
283 (5 %). Hence, the uncertainties in our ambient measurements of formic, acetic and oxalic  
284 acid concentrations were estimated to be 12, 12 and 14 %, respectively.

285 For nitric acid, which was calibrated in post-field laboratory work using a  
286 permeation tube and UV optical absorption, the uncertainty in its ambient concentrations  
287 was estimated to be 13 % based on uncertainties in UV absorption measurements (10 %)  
288 and one standard deviation of the acid's UV absorption signals (3 %),  $^{34}\text{SO}_2$  sensitivity (3  
289 %) and acid's calibrant ion signals (8 %). For propionic acid, which was calibrated in post-  
290 field laboratory work using vapor pressures measured by a capacitance manometer, the  
291 uncertainty in its ambient concentrations was estimated to be 14 % based on the vapor  
292 pressure measurement uncertainty (10 %) and one standard deviation of the  $^{34}\text{SO}_2$   
293 sensitivity (3 %), the acid's calibrant ion signals (8 %) and linear fits of the acid's  
294 calibration curves (3 %). Ambient concentrations and the corresponding uncertainties of  
295 glycolic, valeric and butyric acids were not quantified.

### 296 **2.3. WSOC<sub>g</sub> measurements**

297 WSOC<sub>g</sub> was measured with a MIST chamber coupled to a total organic carbon  
298 (TOC) analyzer (Sievers 900 series, GE Analytical Instruments). Ambient air first passed  
299 through a Teflon filter (45 mm diameter, 2.0  $\mu\text{m}$  pore size, Pall Life Sciences) to remove  
300 particles in the air stream. This filter was changed every 3 to 4 days. The particle-free air  
301 was then pulled into a glass Mist Chamber filled with ultrapure deionized water at a flow  
302 rate of 20 L  $\text{min}^{-1}$ . The MIST chamber scrubbed soluble gases with Henry's law constants  
303 greater than  $10^3 \text{ M atm}^{-1}$  into deionized water (Spaulding et al., 2002). The resulting liquid

304 samples from the MIST chamber were analyzed by the TOC analyzer. The TOC analyzer  
305 converted the organic carbon in the liquid samples to carbon dioxide using UV light and  
306 chemical oxidation. The carbon dioxide formed was then measured by conductivity. The  
307 amount of organic carbon in the liquid samples is proportional to the measured increase in  
308 conductivity of the dissolved carbon dioxide. Each WSOC<sub>g</sub> measurement lasted 4 min.  
309 Background WSOC<sub>g</sub> measurements were performed for 45 min every 12 h by stopping the  
310 sample air flow and rinsing the sampling lines with deionized water. The TOC analyzer  
311 was calibrated using different concentrations of sucrose (as specified by the instrument  
312 manual) before and after the field study. The limit of detection was 0.4 µgC m<sup>-3</sup>. The  
313 measurement uncertainty was estimated to be 10 % based on uncertainties in the sample  
314 air flow, liquid flow and TOC analyzer uncertainty. The MIST chamber and upstream  
315 particle filter were located in an air-conditioned building so were generally below ambient  
316 temperature. Hence, evaporation of collected particles (which will lead to positive artifacts  
317 in WSOC<sub>g</sub> measurements) are not expected to be significant.

#### 318 **2.4. Supporting gas measurements**

319 Supporting gas measurements were provided by a suite of instruments operated by  
320 the SEARCH network. A non-dispersive infrared spectrometer (Thermo Fisher Scientific)  
321 provided hourly CO measurements. A UV absorption analyzer (Thermo Fisher Scientific)  
322 provided hourly O<sub>3</sub> measurements. A gas chromatography-flame ionization detector (GC-  
323 FID, Agilent Technologies) provided hourly VOC measurements.

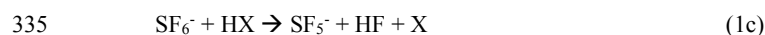
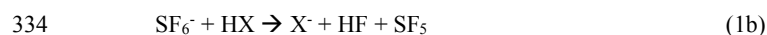
### 324 **3. Results and discussion**

#### 325 **3.1. General SF<sub>6</sub><sup>-</sup> CIMS field performance**

##### 326 **3.1.1. SF<sub>6</sub><sup>-</sup> ion chemistry with organic acids**

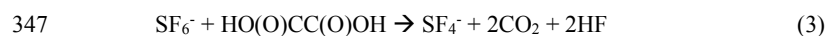
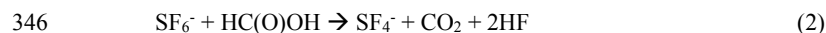
327 CIMS measurements of atmospheric constituents use ion-molecule reactions to  
328 selectively ionize compounds of interest in the complex matrix of ambient air and produce  
329 characteristic ions. The reactions of SF<sub>6</sub><sup>-</sup> with the organic acids (HX) proceed through  
330 reactions 1a to 1c, and gave similar products to those reported previously for SF<sub>6</sub><sup>-</sup> reactions

331 with inorganic acids (Huey et al., 1995):  $SF_5^-$ ,  $X^-$  and  $X\cdot HF$  where  $X^-$  is the conjugate base  
332 of the organic acid (reactions 1a-c).



336 The effective branching ratios of the  $SF_5^-$ ,  $X^-$  and  $X\cdot HF$  product ions can be impacted by  
337 the field strength of the CDC. The  $SF_5^-$  ion (m/z 127, reaction 1c) is a common reaction  
338 product of the reactions of  $SF_6^-$  with many species and is probably thermodynamically  
339 driven by the formation of HF (Huey et al., 1995). Unfortunately, the production of  $SF_5^-$   
340 does not allow for the selective detection of any atmospheric species. In addition, the larger  
341 the branching ratio of the  $SF_5^-$  channel, the lower the CIMS sensitivity is to an individual  
342 acid since the effective rate constants for the  $X^-$  and  $X\cdot HF$  channels are lower.

343 The reaction of  $SF_6^-$  with formic acid and oxalic acid also produced  $SF_4^-$  ions (m/z  
344 108). These reactions are probably thermodynamically driven by the formation of  $CO_2$  and  
345 HF:



348 We used the  $X^-$  and/or  $X\cdot HF$  ions to determine ambient organic acid concentrations  
349 since these ions are characteristic of the individual acids. For all the organic acids, the  $X\cdot$   
350  $HF$  ion signal is substantially lower than that of the  $X^-$  ion for the conditions in this study.  
351 However, this is probably largely due to the relatively high collision energy used in the  
352 CDC, which led to efficient dissociation of the fluoride adducts to form  $X^-$  ions.  
353 Consequently, only the proton transfer channel (1b) is used to quantify most of the organic  
354 acids in the field study. The exceptions are formic and acetic acid as discussed in section  
355 3.2.1 and 3.2.2

356 Table 1 shows a summary of the sensitivities of  $X^-$  and  $X\cdot HF$  ions of some common  
357 atmospheric organic acids. The average sensitivities of the  $HCOO^-$  (m/z 45) and  $HCOO^-$

358 •HF (m/z 65) ions of formic acid were  $1.29 \pm 0.22$  and  $0.29 \pm 0.05$  Hz ppt<sup>-1</sup>, respectively,  
359 while the average sensitivities of the CH<sub>3</sub>COO<sup>-</sup> (m/z 59) and CH<sub>3</sub>COO•HF (m/z 79) ions  
360 of acetic acid were  $1.46 \pm 0.29$  and  $0.30 \pm 0.06$  Hz ppt<sup>-1</sup>, respectively. A weak <sup>210</sup>Po ion  
361 source (< 1 mCi) was used by SF<sub>6</sub><sup>-</sup>-CIMS instrument during the field study, hence these  
362 sensitivities will be substantially higher if a stronger radioactive source is used. Post-field  
363 laboratory work suggest that the sensitivities may increase by as much as a factor of 5 for  
364 a new commercial 20 mCi <sup>210</sup>Po ion source. [Nevertheless, these sensitivities are compared](#)  
365 [to formic and acetic acid sensitivities measured by a high-resolution time-of-flight](#)  
366 [chemical ionization mass spectrometer \(Aerodyne Research Inc.\) that utilized I<sup>-</sup> reagent](#)  
367 [ions during the field study. Only the formic and acetic acid sensitivities were compared](#)  
368 [since laboratory calibrations were not performed to determine the sensitivities for oxalic,](#)  
369 [butyric, glycolic, propionic and valeric acids by I<sup>-</sup>-CIMS. Although the formic acid](#)  
370 [sensitivity measured by I<sup>-</sup>-CIMS \( \$1.33 \pm 0.28\$  Hz ppt<sup>-1</sup>\) was comparable to that measured](#)  
371 [by SF<sub>6</sub><sup>-</sup>-CIMS, the acetic acid sensitivity measured by I<sup>-</sup>-CIMS \(< 0.1 Hz ppt<sup>-1</sup>\) was](#)  
372 [substantially lower than that measured by SF<sub>6</sub><sup>-</sup>-CIMS. Previous studies have similarly](#)  
373 [reported low acetic acid sensitivity measured by I<sup>-</sup>-CIMS \(Aljawhary et al., 2013; Lee et](#)  
374 [al., 2014\).](#)

375 [\\_\\_\\_\\_\\_ Since many recent studies use I<sup>-</sup> as a reagent ion to measure many compounds, the](#)  
376 [measured SF<sub>6</sub><sup>-</sup> sensitivities to organic acids are compared with those of I<sup>-</sup> reported by Lee](#)  
377 [et al. \(2014, 2018\). However, it is important to note that the absolute SF<sub>6</sub><sup>-</sup> and I<sup>-</sup> sensitivities](#)  
378 [values are specific to the respective instruments and their configuration. The sensitivity to](#)  
379 [individual compounds depend on a variety of instrument parameters \(e.g., flow rates,](#)  
380 [pressures, electric fields, ion source activity\) that control ion production and transmission,](#)  
381 [reaction time, declustering efficiency, etc. Consequently, this analysis serves primarily as](#)  
382 [a qualitative comparison of SF<sub>6</sub><sup>-</sup> and I<sup>-</sup> sensitivity.](#)

383 [\\_\\_\\_\\_\\_ Although the I<sup>-</sup> sensitivity to formic acid \( \$2.9\$  Hz ppt<sup>-1</sup>\) reported by Lee et al. \(2014\)](#)  
384 [is higher than that of SF<sub>6</sub><sup>-</sup> \( \$1.29\$  Hz ppt<sup>-1</sup>\), the SF<sub>6</sub><sup>-</sup> sensitivities for the other organic acids](#)  
385 [\(i.e., acetic, oxalic, glycolic and propionic acids\) are substantially higher than those of I<sup>-</sup>](#)  
386 [\(Table S1a\). The SF<sub>6</sub><sup>-</sup> CIMS method is particularly sensitive to oxalic, propionic and](#)  
387 [glycolic acids, which are expected to be present at low concentrations in the atmosphere.](#)



388 [The sensitivities of SF<sub>6</sub><sup>-</sup> and I<sup>-</sup> to SO<sub>2</sub>, HNO<sub>3</sub> and HCl can also be compared \(Table S1b\).](#)  
389 [The SF<sub>6</sub><sup>-</sup> sensitivities of SO<sub>2</sub> and HCl are significantly higher than that of I<sup>-</sup> reported by](#)  
390 [Lee et al. \(2018\). However, I<sup>-</sup> is more sensitive to HNO<sub>3</sub>.](#)

### 391 3.1.2. Characterization of interferences

392 SF<sub>6</sub><sup>-</sup> is very sensitive to many trace atmospheric species but its reactions with water  
393 vapor and O<sub>3</sub> when sampling ambient air can lead to issues both with selectivity and  
394 stability. For example, SF<sub>6</sub><sup>-</sup> reacts nonlinearly with water vapor to form a series of F<sup>-</sup>•(HF)<sub>n</sub>  
395 cluster ions (Huey et al., 1995; Arnold and Viggiano, 2001). SF<sub>6</sub><sup>-</sup> also reacts efficiently  
396 with O<sub>3</sub> to form O<sub>3</sub><sup>-</sup>, which is rapidly converted to CO<sub>3</sub><sup>-</sup> in ambient air (Slusher et al., 2001).  
397 These reactions can deplete SF<sub>6</sub><sup>-</sup> as well as form a variety of potentially interfering ions  
398 from secondary reactions (e.g., F<sup>-</sup>•(HF)<sub>n</sub> and CO<sub>3</sub><sup>-</sup> ions) that depend on more abundant  
399 atmospheric species. For these reasons, efforts were made to minimize interferences by  
400 limiting reaction times and the flow sampled into the CIMS. This was accomplished by  
401 sampling only 0.3 L min<sup>-1</sup> of air through the variable orifice into the flow tube and  
402 maintaining the flow tube at a low pressure (~13 mbar). The 0.3 L min<sup>-1</sup> sampled air flow  
403 is diluted by 3.7 slpm of N<sub>2</sub>/SF<sub>6</sub> flow in the flow tube. The ratio of the sampled air flow to  
404 the N<sub>2</sub>/SF<sub>6</sub> flow introduced into the flow tube is approximately 1:13. While the high N<sub>2</sub>/SF<sub>6</sub>  
405 flow (3.7 slpm) passed through the radioactive source into the flow tube increased the SF<sub>6</sub><sup>-</sup>  
406 reagent ion signal, the high dilution of the sampled air flow in the flow tube reduced the  
407 CIMS instrument sensitivity by decreasing the number density of the analytes.

408 Figure 2 shows a mass spectrum of ambient air. Interference peaks at m/z 39 (F<sup>-</sup>  
409 •(HF) and CO<sub>3</sub><sup>-</sup>, respectively) can be attributed to the presence of water and O<sub>3</sub>,  
410 respectively. The reagent ion <sup>32</sup>SF<sub>6</sub><sup>-</sup> is present at m/z 146. The <sup>32</sup>SF<sub>6</sub><sup>-</sup> reagent ion signal was  
411 saturated, and this caused the sharp drop in the m/z 146 signal as shown in Fig. 2. Since  
412 the <sup>32</sup>SF<sub>6</sub><sup>-</sup> reagent ion signal was saturated for the entire field study, we monitored the ion  
413 signal of its isotope <sup>34</sup>SF<sub>6</sub><sup>-</sup> to determine if the reaction of SF<sub>6</sub><sup>-</sup> with ambient water vapor  
414 (5.92 x 10<sup>-6</sup> to 2.19 x 10<sup>-5</sup> g cm<sup>-3</sup>) and O<sub>3</sub> (2.1 to 82.4 ppb) depleted SF<sub>6</sub><sup>-</sup> reagent ions.  
415 Figure S2a shows the time series of the <sup>34</sup>SF<sub>6</sub><sup>-</sup> ion signal and ambient water vapor  
416 concentration for the entire field study. Despite fluctuations in ambient water vapor and O<sub>3</sub>  
417 concentrations, the <sup>34</sup>SF<sub>6</sub><sup>-</sup> ion signal was relatively constant for the entire field study with

418 a standard deviation of < 3%. This indicates that the reaction of  $\text{SF}_6^-$  with ambient water  
419 vapor and  $\text{O}_3$  did not significantly deplete the  $^{32}\text{SF}_6^-$  reagent ions during the field study.

420 The  $\text{F}_2^{34}\text{SO}_2^-$  ion signal was used to monitor the CIMS  $\text{SO}_2$  sensitivity during the  
421 field study. Figure S2b shows the time series of the  $\text{F}_2^{34}\text{SO}_2^-/^{34}\text{SF}_6^-$  ion signal ratio obtained  
422 in calibration measurements. There is a ~50 % increase in the  $\text{F}_2^{34}\text{SO}_2^-/^{34}\text{SF}_6^-$  ion signal  
423 ratio on 28 Sept 2016, indicating an increase in the CIMS instrument sensitivity. The  
424 increase in CIMS instrument sensitivity is due to the decrease in ambient water vapor  
425 concentrations on 28 Sept 2016 (Fig. S2a). Previous laboratory and field studies showed  
426 that this was due to the hydrolysis of  $\text{F}_2^{34}\text{SO}_2^-$ , which led to the loss of this ion and  
427 diminished sensitivity at higher levels of ambient water vapor (Arnold and Viggiano, 2001;  
428 Slusher et al., 2001). However, the  $\text{SO}_2$  sensitivity at  $\text{F}_2^{34}\text{SO}_2^-$  only varied within a factor  
429 of two for the entire field study with a clear relationship to water vapor (Fig. S2c). The  $\text{SO}_2$   
430 sensitivity did not show any obvious dependence on ambient  $\text{O}_3$  concentrations (Fig. S2d).

431 The formic ( $\text{HCOO}^-$  at  $m/z$  45 and  $\text{HCOO}\cdot\text{HF}$  at  $m/z$  65) and acetic ( $\text{CH}_3\text{COO}^-$   
432  $\cdot\text{HF}$  at  $m/z$  79) acid ions did not show any obvious dependence on ambient water vapor  
433 and  $\text{O}_3$  concentrations during calibration measurements (Fig. S3). Therefore, we do not  
434 expect the sensitivities of the  $\text{X}^-$  and  $\text{X}\cdot\text{HF}$  ions of the studied organic acids to depend on  
435 ambient water vapor and  $\text{O}_3$  concentrations. We accounted for water vapor dependence of  
436 the  $\text{F}_2^{34}\text{SO}_2^-$  ion signal using the linear relationship between the  $\text{F}_2^{34}\text{SO}_2^-$  ion sensitivity  
437 and ambient water vapor concentration (Fig. S2c) in our post-field calibrations, where the  
438 response of the CIMS acid signals were measured relative to the of the  $^{34}\text{SO}_2$  sensitivity.

### 439 3.1.3. Background and calibration measurements

440 Figure S4 shows an example of the CIMS instrument response during the switch  
441 between background, calibration and ambient measurements of formic and acetic acids  
442 during the field study. The 13 s time resolution data was used to determine the CIMS  
443 instrument time response. Formic ( $m/z$  45, 65 and 108) and acetic ( $m/z$  79) acid ion signals  
444 took ~1.5 min to reach a steady state after switches between ambient, calibration and  
445 background measurements (Figs. S4a and S4c).

446 The CIMS time response to a compound is governed primarily by the compound's  
447 propensity to adhere to surfaces. The decays in the formic and acetic acid ion signals and  
448 times required for them to reach steady state after the removal of calibration gases during  
449 the switch from standard addition calibration to ambient sampling were used to determine  
450 the CIMS response time. The signal decays were fitted using double exponential functions.  
451 For formic acid, the m/z 45, 65 and 108 ion signals decayed to  $1/e^2$  in  $37 \pm 2$ ,  $33 \pm 2$  and  
452  $32 \pm 2$  s, respectively (Fig. S4b). For acetic acid, the m/z 79 ion signal decayed to  $1/e^2$  in  
453  $42 \pm 2$  s (Fig. S4d).

## 454 3.2. Ambient measurements

### 455 3.2.1. Formic acid

456 Figure 2 shows typical mass spectra obtained under background and measurement  
457 modes during the field study. The  $SF_6^-$  reagent ion is present at m/z 146. One of the  
458 prominent species in the mass spectrum is formic acid, which is detected as  $HCOO^-$  and  
459  $HCOO \cdot HF$  at m/z 45 and 65, respectively. Our laboratory studies demonstrated that the  
460 reaction of formic acid with  $SF_6^-$  also produced a large fraction of  $SF_4^-$  ions at m/z 108.  
461 The reaction of  $SF_6^-$  with oxalic acid also produced  $SF_4^-$  ions, but its  $SF_4^-$  product ion yield  
462 is low and gas phase oxalic acid is not present in large concentrations. In addition,  $SF_4^-$  is  
463 present in the mass spectrum obtained under background mode but the  $SF_4^-$  background  
464 ion signals are lower than those typically observed in measurement mode at the Yorkville  
465 site. As a result, we determined the ambient formic acid concentrations using the  $HCOO^-$ ,  
466  $HCOO \cdot HF$  and  $SF_4^-$  ions. Figure 3a shows a scatter plot comparing the ambient formic  
467 acid concentrations measured at Yorkville using the  $HCOO^-$ ,  $HCOO \cdot HF$  and  $SF_4^-$  ions.  
468 Linear regression analysis reveals that the formic acid concentrations determined by the  
469 three ions are highly correlated ( $R^2 = 0.99$ ) with slopes exhibiting a near 1:1 correlation.  
470 The excellent correlation between these three ions and the agreement with laboratory data  
471 indicates that formic acid is selectively measured by this method.

472 The time series of formic acid, temperature and solar radiation measured at  
473 Yorkville are shown in Fig. 3b. Formic acid concentrations ranged from 40 ppt to 4 ppb  
474 during the field study, with strong and consistent diurnal trends. The day-to-day variability

475 in formic acid concentrations are associated with changes in solar radiation and  
476 temperature. Higher formic acid concentrations are measured during warm and sunny days,  
477 similar to formic acid measurements performed in Centreville, rural Alabama during the  
478 2013 Southern Oxidant Aerosol Study (SOAS) (Brophy and Farmer, 2015; Millet et al.,  
479 2015). Figure 3c shows the study-averaged diurnal profiles of formic acid and solar  
480 irradiance. Formic acid started to increase at 7:30, which coincided with a sharp increase  
481 in solar irradiance. Concentrations continued to increase throughout the day and peaked at  
482 18:30, which coincided with the approximate time just before solar irradiance reached zero.  
483 Formic acid then decreased continuously throughout the night.

484 The immediate early-morning increase in formic acid observed in this field study  
485 is similar to that seen during the SOAS study (Millet et al., 2015). However, there are some  
486 differences in the formic acid diurnal cycles measured in this field study and the SOAS  
487 study. Formic acid peaked at 15:30 during SOAS, approximately 3 hours before solar  
488 irradiance decreased to zero. In contrast, formic acid concentrations only started to  
489 decrease at sunset (at 19:30) in this study. This suggests that there may be differences in  
490 the types and/or magnitudes of formic acid sources and sinks in this two field studies. Land  
491 cover and/or land use differences may have contributed to differences in formic acid  
492 sources and sinks at the Centreville and Yorkville field sites. The area surrounding the  
493 Yorkville field site is covered primarily by hardwood mixed with farmland and open  
494 pastures. In contrast, the Centreville field site is surrounded by forests comprised of mixed  
495 oak-hickory and loblolly trees (Hansen et al., 2003). It is also possible that seasonal  
496 differences contributed to differences in formic acid sources and sinks in the two field  
497 studies. The SOAS campaign took place in the middle of summer (1 June to 15 July 2013)  
498 when biogenic emissions are typically higher while this field study took place in early fall  
499 when biogenic emissions are lower due to cooler temperatures. For example, the average  
500 concentration of isoprene (a formic acid source) in this study (1.21 ppb) is lower than that  
501 in SOAS (1.92 ppb (Millet et al., 2015)). Despite these differences, our overall results are  
502 similar to the formic acid measurements performed in SOAS in both magnitude and diurnal  
503 variability.

### 504 3.2.2. Acetic acid

505 Acetic acid is detected with  $\text{SF}_6^-$  as  $\text{CH}_3\text{COO}^-$  and  $\text{CH}_3\text{COO}\cdot\text{HF}$  at  $m/z$  59 and 79,  
506 respectively. However, these ions are subject to interferences from the reaction of  $\text{SF}_6^-$  with  
507 water vapor present in the sampled ambient air. Two of these interfering ions  $\text{F}\cdot(\text{HF})_2$  and  
508  $\text{F}\cdot(\text{HF})_3$  occur at  $m/z$  59 and 79, respectively. As discussed earlier, we minimized the  
509 impact of these interferences by diluting the sample flow into the CIMS and running the  
510 CDC at a high collision energy to dissociate the HF cluster ions. As expected from cluster  
511 bond strengths, we found that larger HF cluster ions dissociated more easily than smaller  
512 ones. For example, at a CDC electric field of  $\sim 113 \text{ V cm}^{-1}$  (the configuration used in this  
513 field study), virtually all of the  $\text{F}\cdot(\text{HF})_3$  cluster ions dissociated while very few of the  $\text{F}\cdot$   
514  $\cdot(\text{HF})$  cluster ions dissociated. This indicates that the  $m/z$  79 channel for acetic acid is more  
515 immune to interference from water vapor than the  $m/z$  59 channel. This is supported by the  
516 observation that the background ion signal at  $m/z$  59 ( $R^2 = 0.50$ ) is more highly correlated  
517 with ambient water vapor concentrations than the background ion signal of  $m/z$  79 ( $R^2 =$   
518  $0.30$ ). In addition, the  $m/z$  59 ion is subjected to interference from the reaction of  $\text{SF}_6^-$  with  
519  $\text{O}_3$  present in the sampled ambient air.  $\text{SF}_6^-$  reacts with  $\text{O}_3$  in the presence of  $\text{CO}_2$  to form  
520  $\text{CO}_3^-$  at  $m/z$  60 (Slusher et al., 2001). As shown in Fig. 2, the large  $\text{CO}_3^-$  peak at  $m/z$  60 is  
521 a potential interference to the  $m/z$  59 signal. As the background scrubber also removed  $\text{O}_3$   
522 from the ambient air, there is a large difference in the  $m/z$  60 ion signal between the  
523 measurement and background modes ( $\sim 100\,000 \text{ Hz}$ ). Thus, even a few percent bleed over  
524 of  $m/z$  60 to  $m/z$  59 can lead to an over-estimation of ambient acetic acid concentrations.  
525 For these reasons, we used  $m/z$  79 ( $\text{X}\cdot\text{HF}$ ) to determine ambient acetic acid concentrations  
526 even though this channel has a lower sensitivity than the  $m/z$  59 channel ( $\text{X}^-$ ).

527 The time series of acetic acid, temperature and solar radiation measured at  
528 Yorkville are shown in Fig. 4a. Acetic acid concentrations ranged from 30 ppt to 3 ppb  
529 during the field study. The day-to-day variability in acetic acid concentrations resembled  
530 the behavior of formic acid concentrations, with higher concentrations being measured  
531 during warm and sunny days. Figure 4b shows the study-averaged diurnal profiles of acetic  
532 acid and solar irradiance. The diurnal profile of acetic acid is similar to that of formic acid  
533 with a more pronounced evening maximum. Acetic acid started to increase at 7:30 and  
534 built up through the day, peaking at 19:30 and decreased continuously overnight. In  
535 general, acetic acid concentrations are well correlated with ( $R^2 = 0.67$ ) and comparable in

536 magnitude (~60 % on average) to formic acid. The study-averaged formic acid/acetic acid  
537 concentration ratio (1.65) is comparable to ratios from previous field studies in rural and  
538 urban environments (Talbot et al., 1988; Talbot et al., 1995; Granby et al., 1997; Khare et  
539 al., 1999; Talbot et al., 1999; Baboukas et al., 2000; Singh et al., 2000; Kuhn et al., 2002;  
540 Baasandorj et al., 2015; Millet et al., 2015).

### 541 **3.2.3. Larger organic acids**

542 In addition to formic and acetic acid, eight other ions were monitored during the  
543 field study:  $m/z$  73, 75, 87, 89, 101, 103, 117 and 131. These ions were chosen as they had  
544 significant signals when ambient air was sampled and were not obviously formed from  
545  $SF_6^-$  reaction with water vapor or  $O_3$ . Since the CIMS utilized in this study only had unit  
546 mass resolution, these ions are the sum of all organic acid isomers and isobaric organic  
547 acids of the same molecular weight as well as other product ions from species that might  
548 react with  $SF_6^-$ . We will refer to organic acids with  $m/z$  75, 87, 101, 103, 117 and 131 by  
549 their ion masses. We assign the  $m/z$  73 ion as the  $X^-$  ion of propionic acid because it does  
550 not have organic acid isomers and isobaric species at that  $m/z$ . In addition, real-time ion  
551 chromatography measurements of aerosol composition performed during the field study  
552 demonstrated the presence of particulate oxalic acid (Nah et al., 2018). For this reason, we  
553 assign the  $m/z$  89 ion as the  $X^-$  ion of oxalic acid. As shown in Nah et al. (2018), the gas-  
554 particle ratios of the organic acids depend of their thermodynamic conditions, which are  
555 dependent on the acid's physicochemical properties, ambient temperature, particle water  
556 and pH. Since the measured gas-particle partitioning ratios of oxalic acid (calculated using  
557 the CIMS and ion chromatography measurements) are in good agreement with their  
558 corresponding thermodynamic predictions (Nah et al., 2018), this indicated that our  
559 assignment of the  $m/z$  89 ion to oxalic acid is reasonable. In addition, the high sensitivity  
560 of  $SF_6^-$  to oxalic acid also helps limit interferences due to other acids. Particulate formic  
561 acid and acetic acid were also detected by ion chromatography during the field study, but  
562 were at much lower concentrations relative to the gas phase (Nah et al., 2018).

563 Figures 5 and S5 show the time series and diurnal profiles of oxalic and propionic  
564 acids and organic acids with ions  $m/z$  75, 87, 101, 103, 117 and 131 measured during the  
565 field study. These organic acids displayed very similar day-to-day variability as formic and

566 acetic acids, with higher concentrations (or ion signals) being measured on warm and sunny  
567 days. The diurnal profiles of all the measured organic acids have similar diurnal trends,  
568 with their concentrations (or ion signals) reaching a maximum between 17:30 and 19:30  
569 and rapidly decreasing after sunset.

#### 570 **3.2.4. Comparison with WSOC<sub>g</sub>**

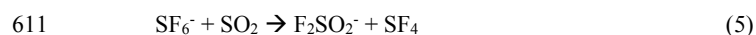
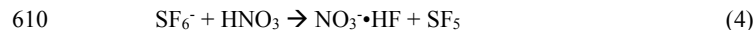
571 WSOC<sub>g</sub> measurements were performed during the field study using a MIST  
572 chamber coupled to a TOC analyzer. The study average WSOC<sub>g</sub> was  $3.6 \pm 2.7 \mu\text{gC m}^{-3}$ ,  
573 slightly lower than that measured during the SOAS study ( $4.9 \mu\text{gC m}^{-3}$ ) (Xu et al., 2017),  
574 and approximately four times lower than that measured in urban Atlanta, Georgia ( $13.7$   
575  $\mu\text{gC m}^{-3}$ ) (Hennigan et al., 2009). Despite being comparable in magnitude, the diurnal  
576 profiles of WSOC<sub>g</sub> measured in this study and the SOAS study are different. WSOC<sub>g</sub>  
577 measured in the SOAS study decreased at sunset, while WSOC<sub>g</sub> measured in this study  
578 decreased 2 hours after sunset. Differences in WSOC<sub>g</sub> concentrations and diurnal profiles  
579 at the three different sites may be due to differences in emission sources as a result of  
580 different measurement periods, land use and/or land cover.

581 To estimate the fraction of WSOC<sub>g</sub> that is comprised of organic acids, the total  
582 organic carbon contributed by formic, acetic, oxalic and propionic acids is compared to the  
583 WSOC<sub>g</sub> measurements. This comparison primarily serves as a check to determine if the  
584 peak assignments are plausible by ensuring that the estimated sum of organic carbon  
585 contributed by these four organic acids is less than or equal to the measured WSOC<sub>g</sub>.  
586 Figures 6a and 6b show the time series and diurnal profiles of WSOC<sub>g</sub> and the organic  
587 carbon contributed by the four organic acids. Formic and acetic acids comprised majority  
588 of the total organic carbon contributed by the four organic acids (study averages of 41 and  
589 54 %, respectively). The carbon mass fraction of WSOC<sub>g</sub> comprised of these four organic  
590 acids ranged from 2 to 100 %. Based on the orthogonal distance regression slope shown in  
591 Fig. 6c, the study-averaged carbon mass fraction of WSOC<sub>g</sub> comprised of the four organic  
592 acids is 22 %. The total organic carbon contributed by the four organic acids are moderately  
593 correlated with WSOC<sub>g</sub> ( $R^2 = 0.42$ ). This is likely due to the presence of other water-soluble  
594 gas phase species (with different day-to-day variability from the organic acids) that  
595 contribute to the WSOC<sub>g</sub>. This is supported by slight differences in the diurnal profiles of

596 WSOC<sub>g</sub> and the organic carbon contributed by the organic acids (Fig. 6b). While the  
597 diurnal profiles of WSOC<sub>g</sub> and the organic carbon contributed by the four organic acids  
598 have similar general shapes, WSOC<sub>g</sub> peaked at 21:30, approximately 2 hours after the solar  
599 irradiance have decreased to zero. In contrast, the organic carbon contributed by the four  
600 organic acids start to decrease at sunset (at 19:30).

### 601 3.2.5. SO<sub>2</sub> and HNO<sub>3</sub> observations

602 In addition to evaluating the field performance of the SF<sub>6</sub><sup>-</sup> CIMS technique in gas-  
603 phase organic acid measurements, another focus of this study was to investigate the  
604 possible sources of the measured organic acids. For this reason, HNO<sub>3</sub> and SO<sub>2</sub> (two  
605 common anthropogenic tracers) were also measured by SF<sub>6</sub><sup>-</sup> CIMS during the field study.  
606 Correlations between the concentrations of organic acids and those of HNO<sub>3</sub> and SO<sub>2</sub> were  
607 then examined to determine if the organic acids were anthropogenic in nature (section 3.3).  
608 While their reactions with SF<sub>6</sub><sup>-</sup> have multiple product channels (Huey et al., 1995), only  
609 the NO<sub>3</sub><sup>-</sup>•HF (m/z 82) and F<sub>2</sub>SO<sub>2</sub><sup>-</sup> (m/z 102) ions were used for quantitative purposes:



612 Figure S6 shows the time series of SO<sub>2</sub> and HNO<sub>3</sub> measured during the field study.  
613 As expected at a rural site, SO<sub>2</sub> and HNO<sub>3</sub> concentrations are low most of the time (study  
614 averages of 230 and 180 ppt, respectively). However, there were occasional periods when  
615 the site was impacted by anthropogenic pollution. In particular, there are spikes in both  
616 SO<sub>2</sub> and HNO<sub>3</sub> concentrations lasting between 1 to 3 hours throughout the study that  
617 corresponded to the site being impacted by power plant or urban emissions. Outside of  
618 these anthropogenic spikes, HNO<sub>3</sub> showed a clear diurnal profile with a maximum at  
619 approximately 12:30, consistent with local photochemical production.

### 620 3.3. Potential sources of organic acids

621 Correlation analysis on organic acid concentrations can provide insights on their  
622 sources. Figure 7 shows that the concentration of formic acid is strongly correlated with  
623 those of the other measured organic acids (R<sup>2</sup> = 0.68 to 0.89). This suggests that these



624 organic acids have the same or similar sources at Yorkville. The sources of organic acids  
625 can be biogenic or anthropogenic in nature. To determine if the primary sources of organic  
626 acids are of biogenic or anthropogenic origin, we first examined the correlations of organic  
627 acid concentrations with those of anthropogenic pollutants CO, SO<sub>2</sub>, O<sub>3</sub> and HNO<sub>3</sub>. CO  
628 and SO<sub>2</sub> are common tracers for combustion sources. The organic acid concentrations (or  
629 ion signals) are poorly correlated with CO (Fig. S7, R<sup>2</sup> = 0.04 to 0.15) and SO<sub>2</sub> (Fig. S8,  
630 R<sup>2</sup> = 0.01 to 0.23), indicating that primary emissions from combustion are a minor source  
631 of organic acids in Yorkville. HNO<sub>3</sub> and O<sub>3</sub> are common photochemical tracers of urban  
632 air masses. The organic acid concentrations (or ion signals) are weakly correlated with O<sub>3</sub>  
633 (Fig. S9, R<sup>2</sup> = 0.11 to 0.31) and HNO<sub>3</sub> (Fig. S10, R<sup>2</sup> = 0.33 to 0.60). In addition, there is  
634 no noticeable increase in organic acid concentrations during periods of elevated CO, SO<sub>2</sub>,  
635 O<sub>3</sub> and HNO<sub>3</sub> concentrations when the site was impacted by pollution plumes. Formic  
636 acid/CO ratios (which have been used in some studies to determine the contribution of  
637 polluted air masses) ranged between  $1.0 \times 10^{-3}$  to  $2.5 \times 10^{-2}$  ppb ppb<sup>-1</sup>. The ratio peaked  
638 consistently in the mid-afternoon, which coincided with when formic acid and CO reached  
639 their maximum and minimum, respectively. In addition, there were no spikes in the formic  
640 acid/CO ratio during the study, suggesting that contributions of polluted air masses to the  
641 daily increase in formic acid are minimal. Together, these results indicate that the primary  
642 sources of organic acids in Yorkville are likely not anthropogenic in nature.

643 Diurnal profiles of the measured organic acids suggest that their sources are linked  
644 to higher daytime temperatures and/or photochemical processes. Figure 8 compares the  
645 concentrations (or ion signals) of organic acids against ambient temperatures measured  
646 during the study. Since there was a noticeable decrease in mean ambient temperatures  
647 starting on 28 Sept 2016, we grouped the datasets into two time periods (3 to 27 Sept and  
648 28 Sept to 12 Oct) to better evaluate the effect of temperature on organic acid  
649 concentrations. The average temperature in the first time period (3 to 27 Sept) is 24.8 °C  
650 (32.6 °C max, 18.1 °C min), while the average temperature in the second time period (28  
651 Sept to 12 Oct) is 19.5 °C (28.4 °C max, 9.5 °C min). We find that organic acid  
652 concentrations are on average higher and more highly correlated with temperatures in the  
653 warmer first time period (R<sup>2</sup> = 0.40 to 0.61) compared to the cooler second time period (R<sup>2</sup>

654 = 0.18 to 0.55). These observations can be explained by temperature-dependent emissions  
655 of organic acids and their BVOC precursors. Previous studies have shown that emissions  
656 of organic acids and their BVOC precursors depend strongly on light and temperature, with  
657 substantially lower concentrations being emitted in the dark and/or at low temperatures  
658 (Kesselmeier et al., 1997; Kesselmeier, 2001; Sindelarova et al., 2014). We find that the  
659 concentration of isoprene, which was the dominant BVOC in Yorkville, has a somewhat  
660 similar diurnal profile as the organic acids and decreased with temperature on 28 Sept 2016  
661 (Fig. S11). In addition, the concentrations of formic and acetic acids are moderately  
662 correlated with that of isoprene ( $R^2 = 0.42$  and  $0.40$ , respectively) (Fig. S12).

663         Multiphase photochemical aging of ambient organic aerosols can also be a source  
664 of gas-phase organic acids (Eliaison et al., 2003; Ervens et al., 2004; Molina et al., 2004;  
665 Lim et al., 2005; Park et al., 2006; Walser et al., 2007; Sorooshian et al., 2007; Vlasenko  
666 et al., 2008; Pan et al., 2009; Sorooshian et al., 2010). Organic acids may be formed in the  
667 particle phase during organic aerosol photochemical aging, with subsequent volatilization  
668 into the gas phase. Real-time ion chromatography measurements of aerosol composition  
669 demonstrated the presence of particulate formic, acetic, oxalic, malonic, succinic and  
670 glutaric acids (Nah et al., 2018). However, since the ratios of gas-phase formic and acetic  
671 acid mass concentration to the total organic aerosol mass concentration are large (study  
672 averages of 40 and 35 %, respectively) (Nah et al., 2018), it is unlikely that organic aerosol  
673 photochemical aging is a large source of formic and acetic acids. In contrast, the ratios of  
674 gas-phase oxalic, malonic, succinic and glutaric acids mass concentration to the total  
675 organic aerosol mass concentration are expected to be small, suggesting that organic  
676 aerosol photochemical aging may be an important source of these gas-phase organic acids.

677         In summary, the temperature dependence and diurnal profile of organic acid  
678 concentrations combined with poor correlations between organic acid concentrations and  
679 those of anthropogenic pollutants CO, SO<sub>2</sub>, O<sub>3</sub> and HNO<sub>3</sub> strongly suggest that the primary  
680 sources of gas-phase organic acids at Yorkville are biogenic in nature. However, our data  
681 alone does not allow us to determine if the organic acids are a result of direct emissions or  
682 photochemical oxidation of other BVOC emissions and/or organic aerosols. Partitioning

683 of these organic acids between the gas and particle phases is discussed in another paper  
684 (Nah et al., 2018).

#### 685 **4. Summary**

686  $\text{SF}_6^-$  reacted with all of the studied organic acids to produce product ions that were  
687 characteristic of the individual acids (i.e.,  $\text{X}^-$  or  $\text{X}\cdot\text{HF}$ ). These reactions all occurred at less  
688 than the maximum collisional rate due to significant yields of  $\text{SF}_5^-$  and  $\text{SF}_4^-$ , which reduced  
689 the sensitivity of the method. For the conditions employed in this study, the sensitivities of  
690  $\text{X}^-$  and  $\text{X}\cdot\text{HF}$  ions of the organic acids ranged from 0.12 to 6.38 Hz ppt<sup>-1</sup>. The detection  
691 limits of the organic acids were approximated from 3 times the standard deviation values  
692 ( $3\sigma$ ) of the ion signals obtained during background measurements. Limits of detection  
693 ranged from 1 to 60 ppt for 2.5 min integration periods for the organic acids studied. It  
694 should be noted that the  $\text{SF}_6^-$  CIMS method is particularly sensitive to oxalic, propionic  
695 and glycolic acids, which are expected to be present at low concentrations in the  
696 atmosphere. Water vapor and  $\text{O}_3$  can lead to interferences with this method but for the  
697 conditions employed in this study, they were largely limited to acetic acid measurements  
698 at  $m/z$  59. However, fluctuations in ambient water vapor can also lead to changes in  
699 sensitivity for the detection of some species (e.g.,  $\text{SO}_2$ ). Uncertainties in organic acid  
700 concentrations originate primarily from calibration measurements and ranged from 12 to  
701 14 %. Overall, the tractable mass spectra obtained by the  $\text{SF}_6^-$  CIMS method coupled with  
702 reasonable limits of detection and the high correlations observed between the individual  
703 organic acids demonstrated the potential of this method. Obvious next steps for the  $\text{SF}_6^-$   
704 CIMS method are to compare it to other measurement methods for organic acids and to  
705 deploy the  $\text{SF}_6^-$  ion chemistry to a higher resolution time-of-flight mass spectrometer to  
706 reduce the potential for interferences.

707 The  $\text{SF}_6^-$  CIMS method was deployed for measurements of gas phase organic acids  
708 in a mixed forest-agricultural area in Yorkville, Georgia from Sept to Oct 2016. The  
709 organic acids measured in the field study were formic, acetic, propionic and oxalic acids.  
710 Ambient concentrations of these organic acids ranged from a few ppt to several ppb. All  
711 the organic acids exhibited similar strong diurnal trends. Organic acid concentrations built  
712 up throughout the day, peaked between 17:30 and 19:30 before decreasing continuously

713 overnight. Strong correlations between organic acid concentrations indicated that these  
714 organic acids likely have the same or similar sources at Yorkville. We concluded that the  
715 organic acids were likely not due to anthropogenic emissions since they were poorly  
716 correlated with anthropogenic pollutants and their concentrations were not elevated when  
717 the site was impacted by pollution plumes. Higher organic acid concentrations were  
718 measured during warm and sunny days. Organic acid concentrations were strongly  
719 correlated with temperature during the first month of the study when ambient temperatures  
720 were high. Together, our results suggested that the primary sources of organic acids at  
721 Yorkville were biogenic in nature. Direct biogenic emissions of organic acids and/or their  
722 BVOC precursors were likely enhanced at high ambient temperatures, resulting in the  
723 observed variability of organic acid concentrations. Another potential source is the  
724 production of organic acids in the particle phase from the multiphase photochemical aging  
725 of organic aerosols followed by evaporation to the gas phase, though this source is likely  
726 not a large source of formic and acetic acids. However, given the inability of current models  
727 and photochemical mechanisms to explain formic acid observations in the Southeastern  
728 U.S. (Millet et al., 2015), it is unlikely that our observations of formic acid and larger  
729 organic acids can be explained as well. Further work (i.e., laboratory, field and modeling  
730 studies) is needed to determine how organic acids are formed in the atmosphere.

## 731 **5. Acknowledgements**

732 The authors thank Eric Edgerton (Atmospheric Research and Analysis, Inc.) for  
733 providing CO, O<sub>3</sub> and VOC measurements and meteorological data. [We also thank Young](#)  
734 [Ro Lee for performing laboratory experiments to determine SF<sub>6</sub><sup>-</sup> sensitivity to HCl.](#)

## 735 **6. Funding**

736 This publication was developed under US Environmental Protection Agency (EPA)  
737 STAR Grant R835882 awarded to Georgia Institute of Technology. It has not been  
738 formally reviewed by the EPA. The views expressed in this document are solely those of  
739 the authors and do not necessarily reflect those of the EPA. EPA does not endorse any  
740 products or commercial services mentioned in this publication.

## 741 **7. Competing financial interests**

742 The authors declare no competing financial interests.

743 **8. Data availability**

744 Data can be accessed by request (greg.huey@eas.gatech.edu).

745 **9. References**

746 Acree, W., and Chickos, J. S.: Phase Transition Enthalpy Measurements of Organic and  
747 Organometallic Compounds. Sublimation, Vaporization and Fusion Enthalpies From 1880  
748 to 2010, *J. Phys. Chem. Ref. Data*, 39, 942, 10.1063/1.3309507, 2010.

749 Aljawhary, D., Lee, A. K. Y., and Abbatt, J. P. D.: High-resolution chemical ionization  
750 mass spectrometry (ToF-CIMS): application to study SOA composition and processing,  
751 *Atmospheric Measurement Techniques*, 6, 3211-3224, 10.5194/amt-6-3211-2013, 2013.

752 Andreae, M. O., Talbot, R. W., Andreae, T. W., and Harriss, R. C.: Formic and Acetic  
753 Acid over the Central Amazon Region, Brazil. 1. Dry Season, *Journal of Geophysical  
754 Research-Atmospheres*, 93, 1616-1624, 10.1029/JD093iD02p01616, 1988.

755 Arnold, S. T., and Viggiano, A. A.: Turbulent ion flow tube study of the cluster-mediated  
756 reactions of SF<sub>6</sub>- with H<sub>2</sub>O, CH<sub>3</sub>OH, and C<sub>2</sub>H<sub>5</sub>OH from 50 to 500 torr, *J. Phys. Chem.  
757 A*, 105, 3527-3531, 10.1021/jp003967y, 2001.

758 Baasandorj, M., Millet, D. B., Hu, L., Mitroo, D., and Williams, B. J.: Measuring acetic  
759 and formic acid by proton-transfer-reaction mass spectrometry: sensitivity, humidity  
760 dependence, and quantifying interferences, *Atmospheric Measurement Techniques*, 8,  
761 1303-1321, 10.5194/amt-8-1303-2015, 2015.

762 Baboukas, E. D., Kanakidou, M., and Mihalopoulos, N.: Carboxylic acids in gas and  
763 particulate phase above the Atlantic Ocean, *Journal of Geophysical Research-  
764 Atmospheres*, 105, 14459-14471, 10.1029/1999jd900977, 2000.

765 Booth, A. M., Barley, M. H., Topping, D. O., McFiggans, G., Garforth, A., and Percival,  
766 C. J.: Solid state and sub-cooled liquid vapour pressures of substituted dicarboxylic acids

767 using Knudsen Effusion Mass Spectrometry (KEMS) and Differential Scanning  
768 Calorimetry, *Atmos. Chem. Phys.*, 10, 4879-4892, 10.5194/acp-10-4879-2010, 2010.

769 Brophy, P., and Farmer, D. K.: A switchable reagent ion high resolution time-of-flight  
770 chemical ionization mass spectrometer for real-time measurement of gas phase oxidized  
771 species: characterization from the 2013 southern oxidant and aerosol study, *Atmospheric*  
772 *Measurement Techniques*, 8, 2945-2959, 10.5194/amt-8-2945-2015, 2015.

773 Carlton, A. G., Turpin, B. J., Lim, H. J., Altieri, K. E., and Seitzinger, S.: Link between  
774 isoprene and secondary organic aerosol (SOA): Pyruvic acid oxidation yields low volatility  
775 organic acids in clouds, *Geophys. Res. Lett.*, 33, 4, 10.1029/2005gl025374, 2006.

776 Chebbi, A., and Carlier, P.: Carboxylic acids in the troposphere, occurrence, sources, and  
777 sinks: A review, *Atmospheric Environment*, 30, 4233-4249, 10.1016/1352-  
778 2310(96)00102-1, 1996.

779 Crounse, J. D., McKinney, K. A., Kwan, A. J., and Wennberg, P. O.: Measurement of gas-  
780 phase hydroperoxides by chemical ionization mass spectrometry, *Analytical Chemistry*,  
781 78, 6726-6732, 10.1021/ac0604235, 2006.

782 Daubert, T. E., and Danner, R. P.: Physical and thermodynamic properties of pure  
783 chemicals: data compilation, Taylor & Francis, Washington, DC, 1989.

784 Eliason, T. L., Aloisio, S., Donaldson, D. J., Cziczo, D. J., and Vaida, V.: Processing of  
785 unsaturated organic acid films and aerosols by ozone, *Atmospheric Environment*, 37, 2207-  
786 2219, 10.1016/s1352-2310(03)00149-3, 2003.

787 Ervens, B., Feingold, G., Frost, G. J., and Kreidenweis, S. M.: A modeling study of aqueous  
788 production of dicarboxylic acids: 1. Chemical pathways and speciated organic mass  
789 production, *Journal of Geophysical Research-Atmospheres*, 109, 10.1029/2003jd004387,  
790 2004.

791 Ervens, B., Carlton, A. G., Turpin, B. J., Altieri, K. E., Kreidenweis, S. M., and Feingold,  
792 G.: Secondary organic aerosol yields from cloud-processing of isoprene oxidation  
793 products, *Geophys. Res. Lett.*, 35, 10.1029/2007gl031828, 2008.

794 Galloway, J. N., Likens, G. E., Keene, W. C., and Miller, J. M.: The Composition of  
795 Precipitation in Remote Areas of the World, *Journal of Geophysical Research-Oceans and*  
796 *Atmospheres*, 87, 8771-8786, 10.1029/JC087iC11p08771, 1982.

797 Granby, K., Egelov, A. H., Nielsen, T., and Lohse, C.: Carboxylic acids: Seasonal variation  
798 and relation to chemical and meteorological parameters, *Journal of Atmospheric*  
799 *Chemistry*, 28, 195-207, 10.1023/a:1005877419395, 1997.

800 Grosjean, D.: Ambient Levels of Formaldehyde, Acetaldehyde, and Formic acid in  
801 Southern Californic- Results of a One-year Base-line Study, *Environmental Science &*  
802 *Technology*, 25, 710-715, 10.1021/es00016a016, 1991.

803 Hansen, D. A., Edgerton, E. S., Hartsell, B. E., Jansen, J. J., Kandasamy, N., Hidy, G. M.,  
804 and Blanchard, C. L.: The southeastern aerosol research and characterization study: Part 1-  
805 overview, *Journal of the Air & Waste Management Association*, 53, 1460-1471, 2003.

806 Hartmann, W. R., Santana, M., Hermoso, M., Andreae, M. O., and Sanhueza, E.: Diurnal  
807 Cycles of Formic and Acetic Acids in the Northern Part of the Guayana Sheld, Venezuela,  
808 *Journal of Atmospheric Chemistry*, 13, 63-72, 10.1007/bf00048100, 1991.

809 Hennigan, C. J., Bergin, M. H., Russell, A. G., Nenes, A., and Weber, R. J.: Gas/particle  
810 partitioning of water-soluble organic aerosol in Atlanta, *Atmos. Chem. Phys.*, 9, 3613-  
811 3628, 10.5194/acp-9-3613-2009, 2009.

812 Huey, L. G., Hanson, D. R., and Howard, C. J.: Reactions of SF<sub>6</sub>- and I- with Atmospheric  
813 Trace Gases, *Journal of Physical Chemistry*, 99, 5001-5008, 10.1021/j100014a021, 1995.

814 Huey, L. G., Tanner, D. J., Slusher, D. L., Dibb, J. E., Arimoto, R., Chen, G., Davis, D.,  
815 Buhr, M. P., Nowak, J. B., Mauldin, R. L., Eisele, F. L., and Kosciuch, E.: CIMS  
816 measurements of HNO<sub>3</sub> and SO<sub>2</sub> at the South Pole during ISCAT 2000, *Atmospheric*  
817 *Environment*, 38, 5411-5421, 10.1016/j.atmosenv.2004.04.037, 2004.

818 Kawamura, K., Ng, L. L., and Kaplan, I. R.: Determination of Organic Acids (C<sub>1</sub>-C<sub>10</sub>) in  
819 the Atmosphere, Motor Exhausts, and Engine Oils, *Environmental Science & Technology*,  
820 19, 1082-1086, 10.1021/es00141a010, 1985.

821 Keene, W. C., Galloway, J. N., and Holden, J. D.: Measurement of Weak Organic Acidity  
822 in Precipitation from Remote Areas of the World, *Journal of Geophysical Research-Oceans*  
823 and *Atmospheres*, 88, 5122-5130, 10.1029/JC088iC09p05122, 1983.

824 Keene, W. C., and Galloway, J. N.: Organic Acidity in Precipitation of North America,  
825 *Atmospheric Environment*, 18, 2491-2497, 10.1016/0004-6981(84)90020-9, 1984.

826 Kesselmeier, J., Bode, K., Hofmann, U., Muller, H., Schafer, L., Wolf, A., Ciccioli, P.,  
827 Brancaleoni, E., Cecinato, A., Frattoni, M., Foster, P., Ferrari, C., Jacob, V., Fugit, J. L.,  
828 Dutaur, L., Simon, V., and Torres, L.: Emission of short chained organic acids, aldehydes  
829 and monoterpenes from *Quercus ilex* L. and *Pinus pinea* L. in relation to physiological  
830 activities, carbon budget and emission algorithms, *Atmospheric Environment*, 31, 119-133,  
831 10.1016/s1352-2310(97)00079-4, 1997.

832 Kesselmeier, J.: Exchange of short-chain oxygenated volatile organic compounds (VOCs)  
833 between plants and the atmosphere: A compilation of field and laboratory studies, *Journal*  
834 *of Atmospheric Chemistry*, 39, 219-233, 10.1023/a:1010632302076, 2001.

835 Khare, P., Kumar, N., Kumari, K. M., and Srivastava, S. S.: Atmospheric formic and acetic  
836 acids: An overview, *Reviews of Geophysics*, 37, 227-248, 10.1029/1998rg900005, 1999.

837 Kim, S., Huey, L. G., Stickel, R. E., Tanner, D. J., Crawford, J. H., Olson, J. R., Chen, G.,  
838 Brune, W. H., Ren, X., Leshner, R., Wooldridge, P. J., Bertram, T. H., Perring, A., Cohen,  
839 R. C., Lefer, B. L., Shetter, R. E., Avery, M., Diskin, G., and Sokolik, I.: Measurement of  
840 HO<sub>2</sub>NO<sub>2</sub> in the free troposphere during the intercontinental chemical transport experiment  
841 - North America 2004, *Journal of Geophysical Research-Atmospheres*, 112,  
842 10.1029/2006jd007676, 2007.

843 Kuhn, U., Rottenberger, S., Biesenthal, T., Ammann, C., Wolf, A., Schebeske, G., Oliva,  
844 S. T., Tavares, T. M., and Kesselmeier, J.: Exchange of short-chain monocarboxylic acids  
845 by vegetation at a remote tropical forest site in Amazonia, *Journal of Geophysical*  
846 *Research-Atmospheres*, 107, 18, 10.1029/2000jd000303, 2002.



847 Lee, B. H., Lopez-Hilfiker, F. D., Mohr, C., Kurten, T., Worsnop, D. R., and Thornton, J.  
848 A.: An Iodide-Adduct High-Resolution Time-of-Flight Chemical-Ionization Mass  
849 Spectrometer: Application to Atmospheric Inorganic and Organic Compounds,  
850 *Environmental Science & Technology*, 48, 6309-6317, 10.1021/es500362a, 2014.

851 Lee, B. H., Lopez-Hilfiker, F. D., Veres, P. R., McDuffie, E. E., Fibiger, D. L., Sparks, T.  
852 L., Ebben, C. J., Green, J. R., Schroder, J. C., Campuzano-Jost, P., Iyer, S., D'Ambro, E.  
853 L., Schobesberger, S., Brown, S. S., Wooldridge, P. J., Cohen, R. C., Fiddler, M. N.,  
854 Bililign, S., Jimenez, J. L., Kurtén, T., Weinheimer, A. J., Jaegle, L., and Thornton, J. A.:  
855 Flight Deployment of a High-Resolution Time-of-Flight Chemical Ionization Mass  
856 Spectrometer: Observations of Reactive Halogen and Nitrogen Oxide Species, *Journal of*  
857 *Geophysical Research: Atmospheres*, 0, doi:10.1029/2017JD028082, 2018.

858 Liao, J., Sihler, H., Huey, L. G., Neuman, J. A., Tanner, D. J., Friess, U., Platt, U., Flocke,  
859 F. M., Orlando, J. J., Shepson, P. B., Beine, H. J., Weinheimer, A. J., Sjostedt, S. J., Nowak,  
860 J. B., Knapp, D. J., Staebler, R. M., Zheng, W., Sander, R., Hall, S. R., and Ullmann, K.:  
861 A comparison of Arctic BrO measurements by chemical ionization mass spectrometry and  
862 long path-differential optical absorption spectroscopy, *Journal of Geophysical Research-*  
863 *Atmospheres*, 116, 10.1029/2010jd014788, 2011.

864 Lide, D. R.: *CRC handbook of chemistry and physics: a ready-reference book of chemical*  
865 *and physical data*, CRC Press, Boca Raton, FL, 1995.

866 Lim, H. J., Carlton, A. G., and Turpin, B. J.: Isoprene forms secondary organic aerosol  
867 through cloud processing: Model simulations, *Environmental Science & Technology*, 39,  
868 4441-4446, 10.1021/es048039h, 2005.

869 Millet, D. B., Baasandorj, M., Farmer, D. K., Thornton, J. A., Baumann, K., Brophy, P.,  
870 Chaliyakunnel, S., de Gouw, J. A., Graus, M., Hu, L., Koss, A., Lee, B. H., Lopez-Hilfiker,  
871 F. D., Neuman, J. A., Paulot, F., Peischl, J., Pollack, I. B., Ryerson, T. B., Warneke, C.,  
872 Williams, B. J., and Xu, J.: A large and ubiquitous source of atmospheric formic acid,  
873 *Atmos. Chem. Phys.*, 15, 6283-6304, 10.5194/acp-15-6283-2015, 2015.

874 Molina, M. J., Ivanov, A. V., Trakhtenberg, S., and Molina, L. T.: Atmospheric evolution  
875 of organic aerosol, *Geophys. Res. Lett.*, 31, 10.1029/2004gl020910, 2004.

876 Nah, T., Guo, H., Sullivan, A. P., Chen, Y., Tanner, D. J., Nenes, A., Russell, A., Ng, N.  
877 L., Huey, L. G., and Weber, R. J.: Characterization of Aerosol Composition, Aerosol  
878 Acidity and Organic Acid Partitioning at an Agriculture-intensive Rural Southeastern U.S.  
879 Site, *Atmos. Chem. Phys. Discuss.*, in review, 10.5194/acp-2018-373, 2018.

880 Neuman, J. A., Ryerson, T. B., Huey, L. G., Jakoubek, R., Nowak, J. B., Simons, C., and  
881 Fehsenfeld, F. C.: Calibration and evaluation of nitric acid and ammonia permeation tubes  
882 by UV optical absorption, *Environmental Science & Technology*, 37, 2975-2981,  
883 10.1021/es0264221, 2003.

884 Nguyen, T. B., Crouse, J. D., Teng, A. P., Clair, J. M. S., Paulot, F., Wolfe, G. M., and  
885 Wennberg, P. O.: Rapid deposition of oxidized biogenic compounds to a temperate forest,  
886 *Proc. Natl. Acad. Sci. U. S. A.*, 112, E392-E401, 10.1073/pnas.1418702112, 2015.

887 Nolte, C. G., Solomon, P. A., Fall, T., Salmon, L. G., and Cass, G. R.: Seasonal and spatial  
888 characteristics of formic and acetic acids concentrations in the southern California  
889 atmosphere, *Environmental Science & Technology*, 31, 2547-2553, 10.1021/es960954i,  
890 1997.

891 Nowak, J. B., Huey, L. G., Russell, A. G., Tian, D., Neuman, J. A., Orsini, D., Sjostedt, S.  
892 J., Sullivan, A. P., Tanner, D. J., Weber, R. J., Nenes, A., Edgerton, E., and Fehsenfeld, F.  
893 C.: Analysis of urban gas phase ammonia measurements from the 2002 Atlanta Aerosol  
894 Nucleation and Real-Time Characterization Experiment (ANARChE), *Journal of*  
895 *Geophysical Research-Atmospheres*, 111, 14, 10.1029/2006jd007113, 2006.

896 Orzechowska, G. E., and Paulson, S. E.: Photochemical sources of organic acids. 1.  
897 Reaction of ozone with isoprene, propene, and 2-butenes under dry and humid conditions  
898 using SPME, *J. Phys. Chem. A*, 109, 5358-5365, 10.1021/jp050166s, 2005.

899 Pan, X., Underwood, J. S., Xing, J. H., Mang, S. A., and Nizkorodov, S. A.:  
900 Photodegradation of secondary organic aerosol generated from limonene oxidation by

901 ozone studied with chemical ionization mass spectrometry, *Atmos. Chem. Phys.*, **9**, 3851-  
902 3865, 10.5194/acp-9-3851-2009, 2009.

903 Park, J., Gomez, A. L., Walser, M. L., Lin, A., and Nizkorodov, S. A.: Ozonolysis and  
904 photolysis of alkene-terminated self-assembled monolayers on quartz nanoparticles:  
905 implications for photochemical aging of organic aerosol particles, *Physical Chemistry*  
906 *Chemical Physics*, **8**, 2506-2512, 10.1039/b602704k, 2006.

907 Paulot, F., Wunch, D., Crouse, J. D., Toon, G. C., Millet, D. B., DeCarlo, P. F.,  
908 Vigouroux, C., Deutscher, N. M., Abad, G. G., Notholt, J., Warneke, T., Hannigan, J. W.,  
909 Warneke, C., de Gouw, J. A., Dunlea, E. J., De Maziere, M., Griffith, D. W. T., Bernath,  
910 P., Jimenez, J. L., and Wennberg, P. O.: Importance of secondary sources in the  
911 atmospheric budgets of formic and acetic acids, *Atmos. Chem. Phys.*, **11**, 1989-2013,  
912 10.5194/acp-11-1989-2011, 2011.

913 Seco, R., Penuelas, J., and Filella, I.: Short-chain oxygenated VOCs: Emission and uptake  
914 by plants and atmospheric sources, sinks, and concentrations, *Atmospheric Environment*,  
915 **41**, 2477-2499, 10.1016/j.atmosenv.2006.11.029, 2007.

916 Sindelarova, K., Granier, C., Bouarar, I., Guenther, A., Tilmes, S., Stavrou, T., Muller,  
917 J. F., Kuhn, U., Stefani, P., and Knorr, W.: Global data set of biogenic VOC emissions  
918 calculated by the MEGAN model over the last 30 years, *Atmos. Chem. Phys.*, **14**, 9317-  
919 9341, 10.5194/acp-14-9317-2014, 2014.

920 Singh, H., Chen, Y., Tabazadeh, A., Fukui, Y., Bey, I., Yantosca, R., Jacob, D., Arnold,  
921 F., Wohlfrom, K., Atlas, E., Flocke, F., Blake, D., Blake, N., Heikes, B., Snow, J., Talbot,  
922 R., Gregory, G., Sachse, G., Vay, S., and Kondo, Y.: Distribution and fate of selected  
923 oxygenated organic species in the troposphere and lower stratosphere over the Atlantic,  
924 *Journal of Geophysical Research-Atmospheres*, **105**, 3795-3805, 10.1029/1999jd900779,  
925 2000.

926 Slusher, D. L., Pitteri, S. J., Haman, B. J., Tanner, D. J., and Huey, L. G.: A chemical  
927 ionization technique for measurement of pernitric acid in the upper troposphere and the  
928 polar boundary layer, *Geophys. Res. Lett.*, **28**, 3875-3878, 10.1029/2001gl013443, 2001.

929 Slusher, D. L., Huey, L. G., Tanner, D. J., Chen, G., Davis, D. D., Buhr, M., Nowak, J. B.,  
930 Eisele, F. L., Kosciuch, E., Mauldin, R. L., Lefer, B. L., Shetter, R. E., and Dibb, J. E.:  
931 Measurements of pernitric acid at the South Pole during ISCAT 2000, *Geophys. Res. Lett.*,  
932 29, 10.1029/2002gl015703, 2002.

933 Sorooshian, A., Ng, N. L., Chan, A. W. H., Feingold, G., Flagan, R. C., and Seinfeld, J.  
934 H.: Particulate organic acids and overall water-soluble aerosol composition measurements  
935 from the 2006 Gulf of Mexico Atmospheric Composition and Climate Study (GoMACCS),  
936 *Journal of Geophysical Research-Atmospheres*, 112, 16, 10.1029/2007jd008537, 2007.

937 Sorooshian, A., Murphy, S. M., Hersey, S., Bahreini, R., Jonsson, H., Flagan, R. C., and  
938 Seinfeld, J. H.: Constraining the contribution of organic acids and AMS m/z 44 to the  
939 organic aerosol budget: On the importance of meteorology, aerosol hygroscopicity, and  
940 region, *Geophys. Res. Lett.*, 37, 5, 10.1029/2010gl044951, 2010.

941 Souza, S. R., and Carvalho, L. R. F.: Seasonality influence in the distribution of formic and  
942 acetic acids in the urban atmosphere of Sao Paulo City, Brazil, *Journal of the Brazilian*  
943 *Chemical Society*, 12, 755-762, 2001.

944 Spaulding, R. S., Talbot, R. W., and Charles, M. J.: Optimization of a mist chamber (cofer  
945 scrubber) for sampling water-soluble organics in air, *Environmental Science &*  
946 *Technology*, 36, 1798-1808, 10.1021/es011189x, 2002.

947 Talbot, R. W., Beecher, K. M., Harriss, R. C., and Cofer, W. R.: Atmospheric  
948 Geochemistry of Formic and Acetic Acids at a Mid-latitude Temperate Site, *Journal of*  
949 *Geophysical Research-Atmospheres*, 93, 1638-1652, 10.1029/JD093iD02p01638, 1988.

950 Talbot, R. W., Mosher, B. W., Heikes, B. G., Jacob, D. J., Munger, J. W., Daube, B. C.,  
951 Keene, W. C., Maben, J. R., and Artz, R. S.: Carboxylic Acids in the Rural Continental  
952 Atmosphere over the Eastern United States during the Shenandoah Cloud and  
953 Photochemistry Experiment, *Journal of Geophysical Research-Atmospheres*, 100, 9335-  
954 9343, 10.1029/95jd00507, 1995.

955 Talbot, R. W., Dibb, J. E., Scheuer, E. M., Blake, D. R., Blake, N. J., Gregory, G. L.,  
956 Sachse, G. W., Bradshaw, J. D., Sandholm, S. T., and Singh, H. B.: Influence of biomass  
957 combustion emissions on the distribution of acidic trace gases over the southern Pacific  
958 basin during austral springtime, *Journal of Geophysical Research-Atmospheres*, 104, 5623-  
959 5634, 10.1029/98jd00879, 1999.

960 Veres, P., Roberts, J. M., Warneke, C., Welsh-Bon, D., Zahniser, M., Herndon, S., Fall, R.,  
961 and de Gouw, J.: Development of negative-ion proton-transfer chemical-ionization mass  
962 spectrometry (NI-PT-CIMS) for the measurement of gas-phase organic acids in the  
963 atmosphere, *Int. J. Mass Spectrom.*, 274, 48-55, 10.1016/j.ijms.2008.04.032, 2008.

964 Veres, P., Roberts, J. M., Burling, I. R., Warneke, C., de Gouw, J., and Yokelson, R. J.:  
965 Measurements of gas-phase inorganic and organic acids from biomass fires by negative-  
966 ion proton-transfer chemical-ionization mass spectrometry, *Journal of Geophysical*  
967 *Research-Atmospheres*, 115, 10.1029/2010jd014033, 2010.

968 Veres, P. R., Roberts, J. M., Cochran, A. K., Gilman, J. B., Kuster, W. C., Holloway, J. S.,  
969 Graus, M., Flynn, J., Lefer, B., Warneke, C., and de Gouw, J.: Evidence of rapid production  
970 of organic acids in an urban air mass, *Geophys. Res. Lett.*, 38, 10.1029/2011gl048420,  
971 2011.

972 Vlasenko, A., George, I. J., and Abbatt, J. P. D.: Formation of volatile organic compounds  
973 in the heterogeneous oxidation of condensed-phase organic films by gas-phase OH, *J. Phys.*  
974 *Chem. A*, 112, 1552-1560, 10.1021/jp0772979, 2008.

975 Walser, M. L., Park, J., Gomez, A. L., Russell, A. R., and Nizkorodov, S. A.:  
976 Photochemical aging of secondary organic aerosol particles generated from the oxidation  
977 of d-limonene, *J. Phys. Chem. A*, 111, 1907-1913, 10.1021/jp0662931, 2007.

978 Xu, L., Guo, H. Y., Weber, R. J., and Ng, N. L.: Chemical Characterization of Water-  
979 Soluble Organic Aerosol in Contrasting Rural and Urban Environments in the Southeastern  
980 United States, *Environmental Science & Technology*, 51, 78-88, 10.1021/acs.est.6b05002,  
981 2017.

982 YataVELLI, R. L. N., Mohr, C., Stark, H., Day, D. A., Thompson, S. L., Lopez-Hilfiker, F.  
983 D., Campuzano-Jost, P., Palm, B. B., Vogel, A. L., Hoffmann, T., Heikkinen, L., Aijala,  
984 M., Ng, N. L., Kimmel, J. R., Canagaratna, M. R., Ehn, M., Junninen, H., Cubison, M. J.,  
985 Petaja, T., Kulmala, M., Jayne, J. T., Worsnop, D. R., and Jimenez, J. L.: Estimating the  
986 contribution of organic acids to northern hemispheric continental organic aerosol,  
987 *Geophys. Res. Lett.*, 42, 6084-6090, 10.1002/2015gl064650, 2015.

988 Zhang, R. Y., Suh, I., Zhao, J., Zhang, D., Fortner, E. C., Tie, X. X., Molina, L. T., and  
989 Molina, M. J.: Atmospheric new particle formation enhanced by organic acids, *Science*,  
990 304, 1487-1490, 10.1126/science.1095139, 2004.

991

992

993

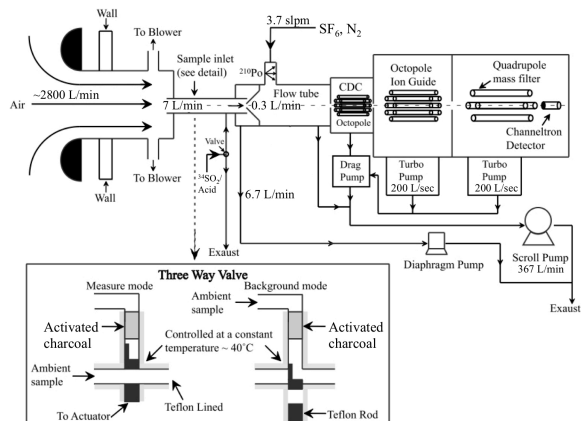
994

995

996

997

998



999

1000 **Figure 1:** The CIMS instrument and inlet configuration used in the field study. The  
 1001 automated three-way sampling valve is shown in the inset. The figure was adapted from  
 1002 Liao et al. (2011).

1003

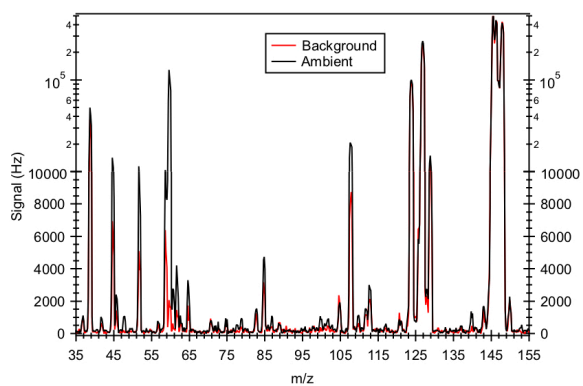
1004

1005

1006

1007

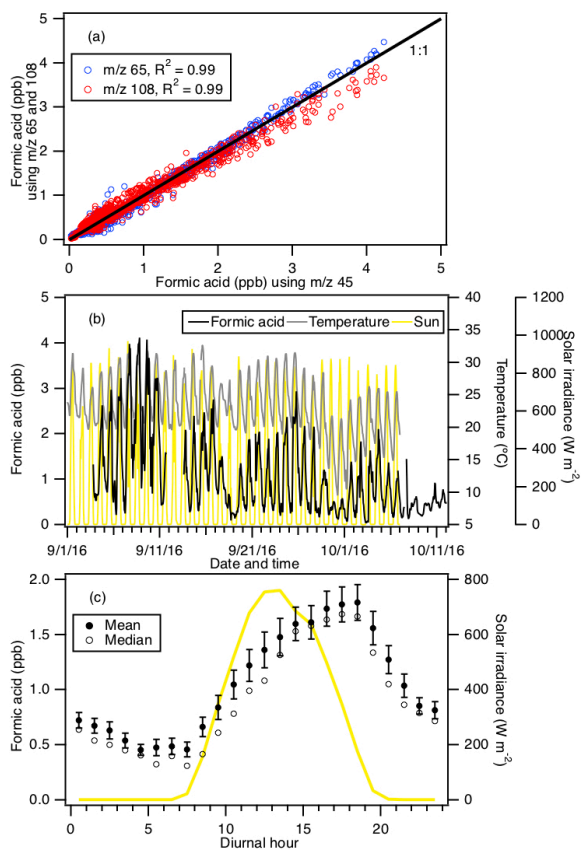
1008



1009

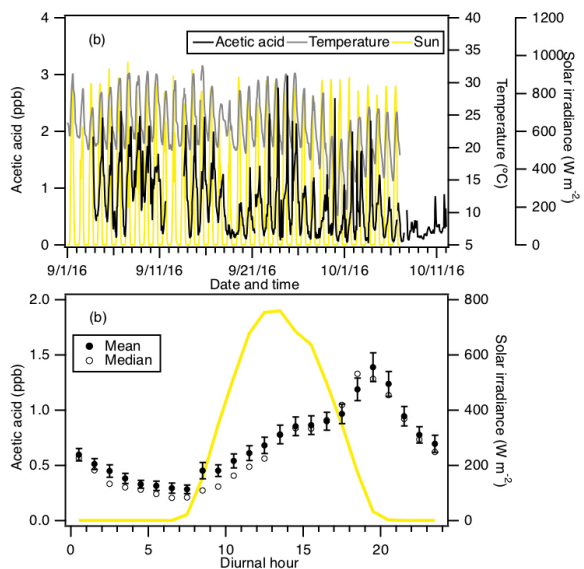
1010 **Figure 2:** Mass spectrum of ambient air and background measured in Yorkville, Georgia  
 1011 on 8 Sept 2016 using SF<sub>6</sub><sup>-</sup>. Note that the <sup>32</sup>SF<sub>6</sub><sup>-</sup> reagent ion signal (at m/z 146) is saturated,  
 1012 causing the sharp drop in its signal. As a result, the ion signal of its isotope <sup>34</sup>SF<sub>6</sub><sup>-</sup> (at m/z  
 1013 150) was monitored to determine if the reaction of SF<sub>6</sub><sup>-</sup> with ambient water vapor and O<sub>3</sub>  
 1014 depleted SF<sub>6</sub><sup>-</sup> reagent ions.





1015

1016 **Figure 3:** (a) Scatter plot comparison of ambient formic acid concentrations determined  
 1017 using mass peaks m/z 45, 65 and 108. The three datasets correlated well with one another  
 1018 ( $R^2 = 0.99$ ). Linear regression of the data gave slopes of 1 (for m/z 65) and 0.95 (for m/z  
 1019 108), indicating that all three mass peaks can be used to determine the formic acid  
 1020 concentration. (b) Time series of formic acid concentration, temperature and solar  
 1021 irradiance. All the data are displayed as 1-hour averages. (c) Diurnal profiles of formic acid  
 1022 concentration (symbols) and solar irradiance (yellow line). All the concentrations represent  
 1023 averages in 1-hour intervals and the standard errors are plotted as error bars.



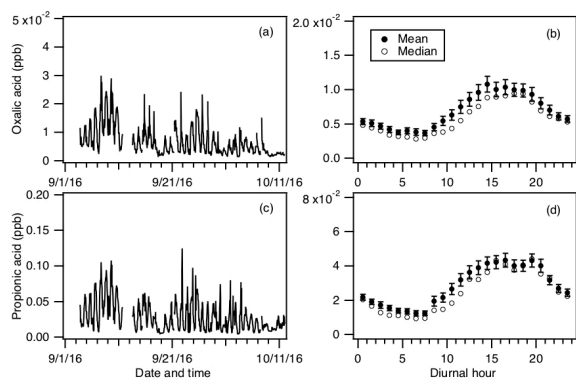
1024

1025 **Figure 4:** (a) Time series of acetic acid concentration, temperature and solar irradiance.  
 1026 All the data are displayed as 1-hour averages. (c) Diurnal profiles of acetic acid (symbols)  
 1027 and solar irradiance (yellow line). All the concentrations represent averages in 1-hour  
 1028 intervals and the standard errors are plotted as error bars.

1029

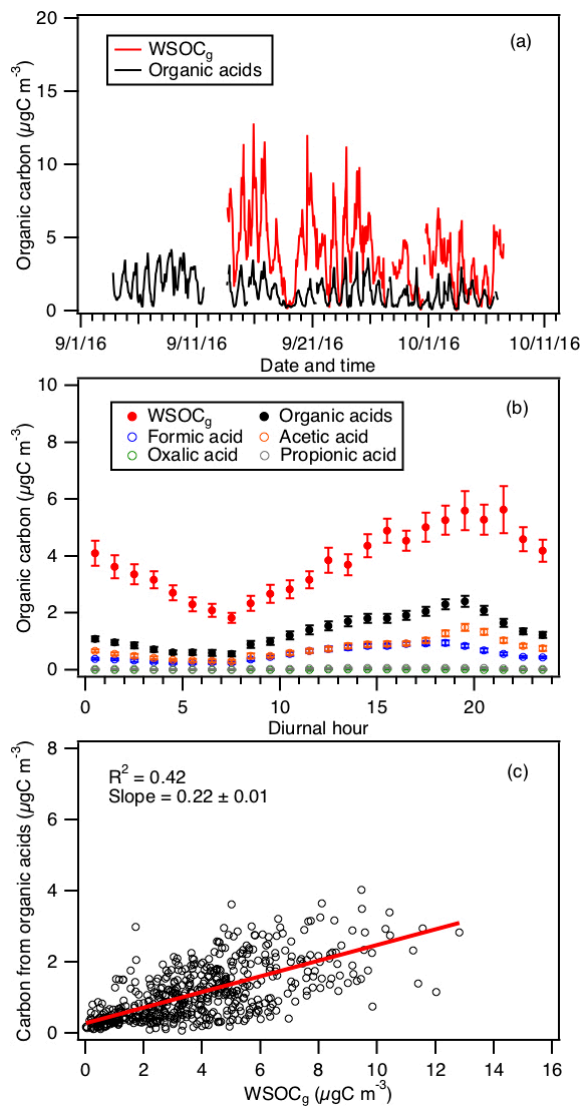
1030

1031



1032

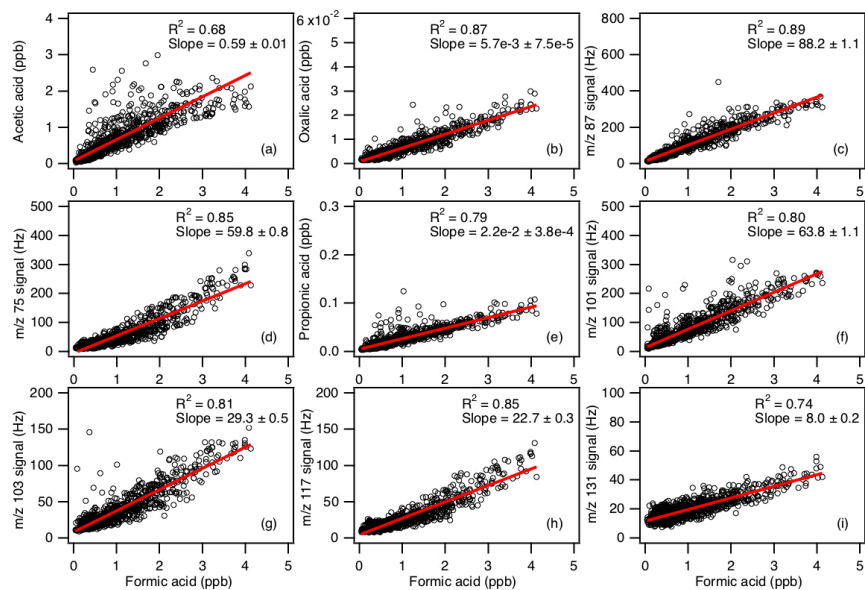
1033 **Figure 5:** Time series of concentrations of (a) oxalic and (c) propionic acids measured  
 1034 during the field study. All the data are displayed as 1-hour averages. Their corresponding  
 1035 diurnal profiles are shown in (b) and (d), respectively. The diurnal profile concentrations  
 1036 represent averages in 1-hour intervals and the standard errors are plotted as error bars.



1037

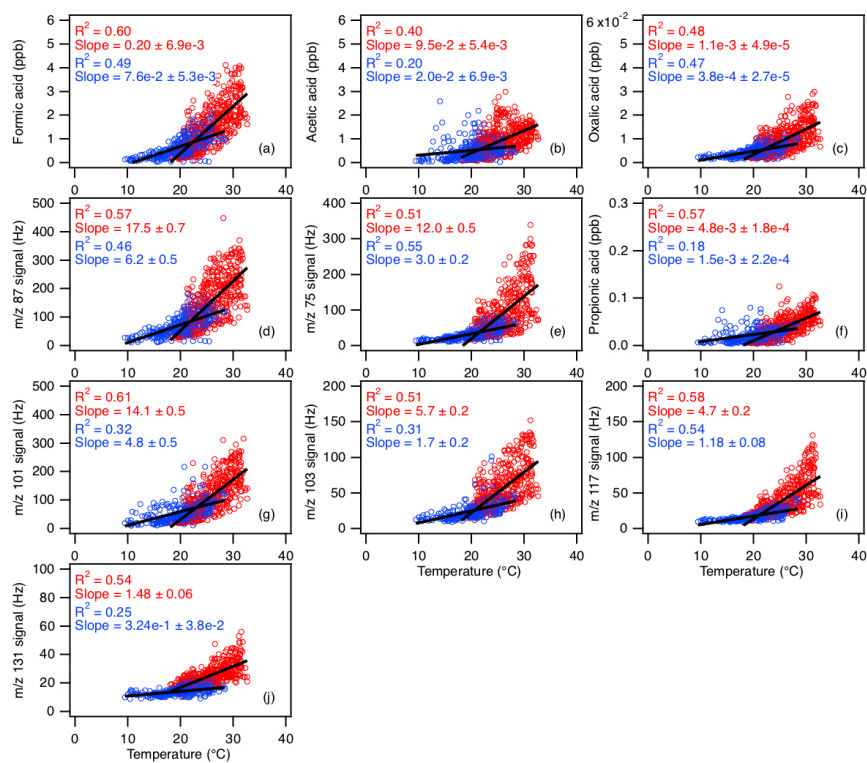
1038 **Figure 6:** (a) Time series of WSOC<sub>g</sub> and the total organic carbon contributed by formic,  
 1039 acetic, oxalic and propionic acids. All the data are displayed as 1-hour averages. (b) Diurnal  
 1040 profiles of WSOC<sub>g</sub> and the total organic carbon contributed by formic, acetic, oxalic and  
 1041 propionic acids. Also shown are the diurnal profiles of the organic carbon contributed by

1042 the individual organic acids. All the concentrations represent the mean hourly averages and  
 1043 the standard errors are plotted as error bars. (c) Scatter plot of total organic carbon  
 1044 contributed by formic, acetic, oxalic and propionic acids with  $WSOC_g$ .



1045

1046 **Figure 7:** Scatter plots of concentrations (or ion signals) of the measured organic acids  
 1047 with formic acid concentration. All the data are displayed as 1-hour averages. Red lines  
 1048 shown are linear fits to the data.



1049

1050 **Figure 8:** Scatter plots of concentrations (or ion signals) of the measured organic acids  
 1051 with ambient temperature. The red symbols are data collected from 3 to 27 Sept, while the  
 1052 blue symbols are data collected from 28 Sept onwards. All the data are displayed as 1-hour  
 1053 averages. Black lines shown are linear fits to the datasets.

1054

1055

1056

1057

1058

1059 **Table 1:** Summary of organic acids of interest, their detection limits and sensitivities of  
 1060 their X<sup>-</sup> and X<sup>-</sup>•HF ions<sup>a</sup>

Organic Acid	Detection limit (ppt) <sup>b</sup>	Sensitivity (Hz ppt <sup>-1</sup> )	
		X <sup>-</sup>	X <sup>-</sup> •HF
Formic acid	30	1.29 ± 0.22	0.29 ± 0.05
Acetic acid	60	1.46 ± 0.29	0.30 ± 0.06
Oxalic acid	1	6.38 ± 0.32	0.97 ± 0.05
Butyric acid	30	0.41 ± 0.01	0.12 ± 0.004
Glycolic acid	2	5.53 ± 0.11	1.64 ± 0.03
Propionic acid	6	2.05 ± 0.02	1.26 ± 0.01
Valeric acid	10	0.76 ± 0.008	0.35 ± 0.004

1061 <sup>a</sup>Only organic acids with calibration measurements are shown.

1062 <sup>b</sup>Detection limits are approximated from 3 times the standard deviation values (3σ) of the  
 1063 ion signals measured during background mode. Shown here are the average detection limits  
 1064 of the organic acids for 2.5 min averaging periods which corresponds to the length of a  
 1065 background measurement at a 4 % duty cycle for each mass.

1 **Supplementary Information:**

2 **Real-time measurements of gas-phase organic acids using SF<sub>6</sub><sup>-</sup> chemical ionization**  
3 **mass spectrometry**

4

5 Theodora Nah,<sup>1,a</sup> Yi Ji,<sup>1,2</sup> David J. Tanner,<sup>1</sup> Hongyu Guo,<sup>1</sup> Amy P. Sullivan,<sup>3</sup> Nga Lee  
6 Ng,<sup>1,2</sup> Rodney J. Weber<sup>1</sup> and L. Gregory Huey<sup>1\*</sup>

7

8 <sup>1</sup>*School of Earth and Atmospheric Sciences, Georgia Institute of Technology, Atlanta, GA, USA*

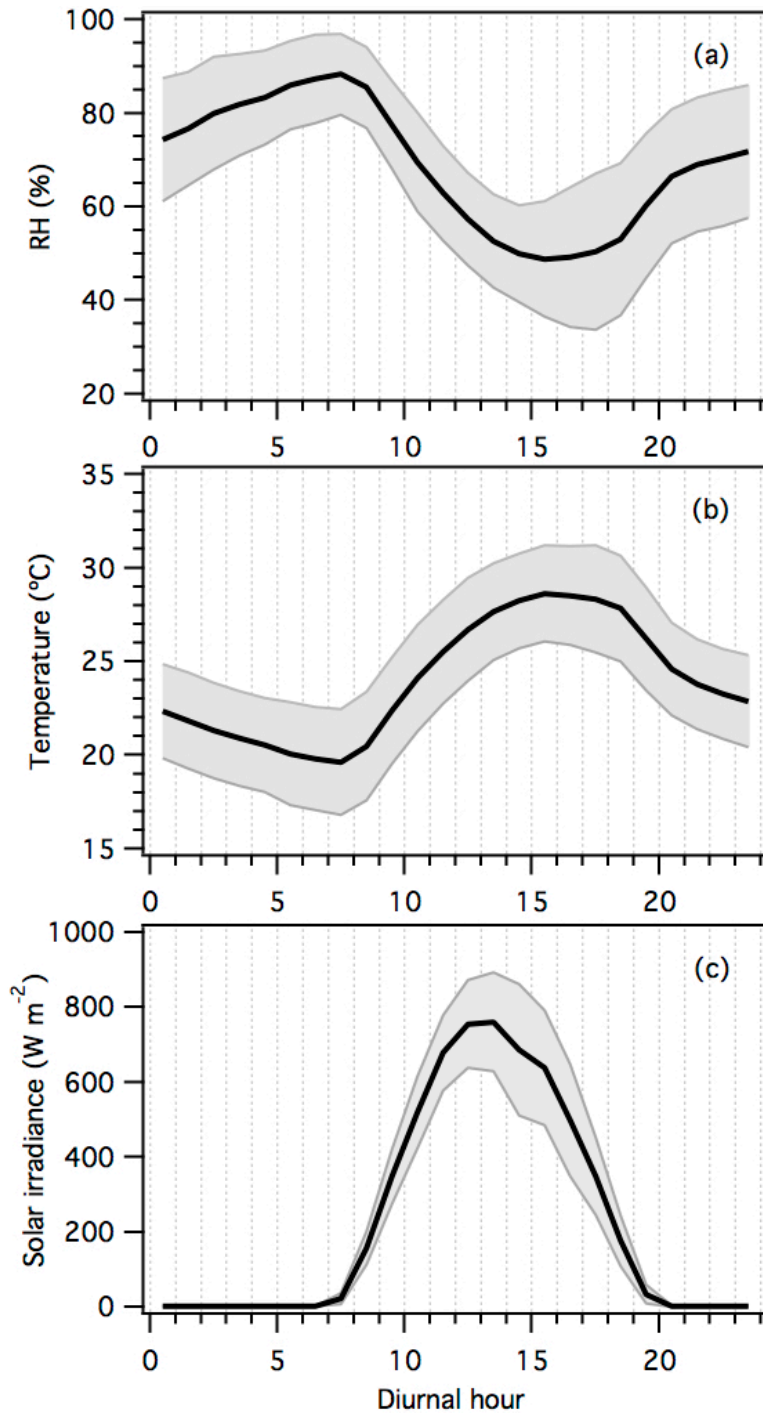
9 <sup>2</sup>*School of Chemical and Biomolecular Engineering, Georgia Institute of Technology, Atlanta, GA, USA*

10 <sup>3</sup>*Department of Atmospheric Science, Colorado State University, Fort Collins, CO, USA*

11 <sup>a</sup>*Now at School of Energy and Environment, City University of Hong Kong, Kowloon, Hong Kong, China*

12 \* *To whom correspondence should be addressed: greg.huey@eas.gatech.edu*



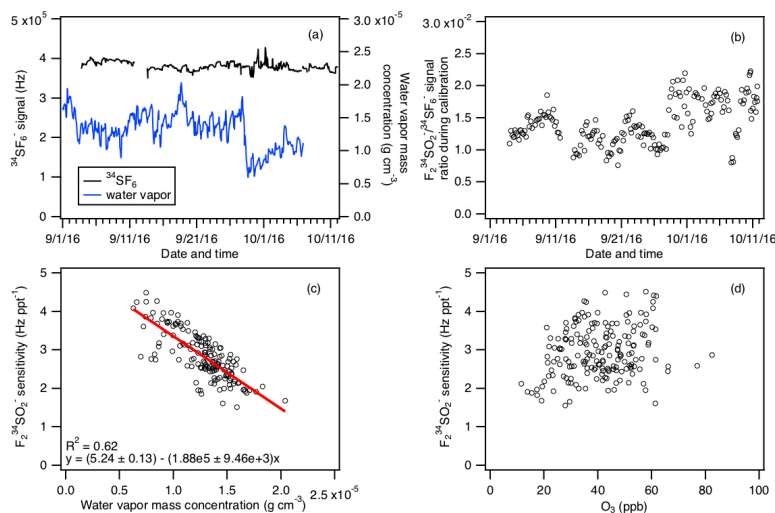


13

14 **Figure S1:** Diurnal trends of (a) relative humidity, (b) temperature, and (c) solar radiance.

15 The lines within the shaded area represents the average values. The upper and lower

16 boundaries of the shaded areas mark one standard deviation.



17

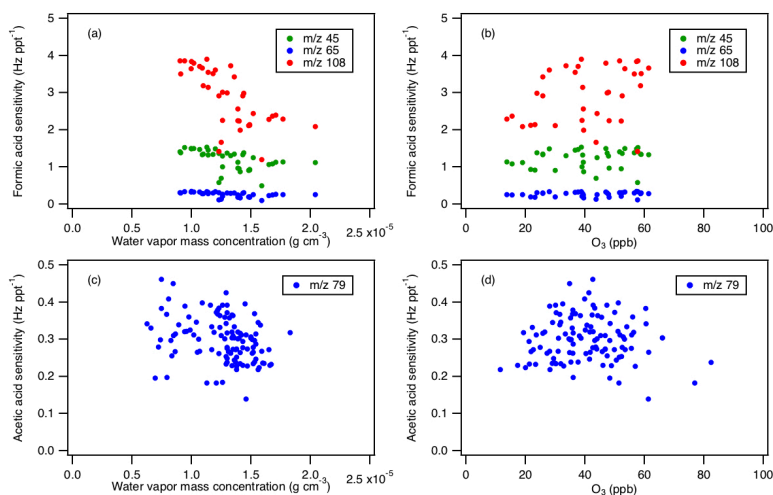
18 **Figure S2:** (a) Time series of <sup>34</sup>SF<sub>6</sub><sup>-</sup> reagent ion signal and ambient water vapor  
 19 concentration for the entire field study. The ambient water vapor mass concentrations are  
 20 determined from ambient relative humidities and temperatures. (b) Time series of F<sub>2</sub><sup>34</sup>SO<sub>2</sub><sup>-</sup>  
 21 /<sup>34</sup>SF<sub>6</sub><sup>-</sup> ion signal ratio obtained during calibration measurements. Panels (c) and (d) show  
 22 the F<sub>2</sub><sup>34</sup>SO<sub>2</sub><sup>-</sup> ion sensitivity obtained from calibration measurements as a function of  
 23 ambient water vapor and O<sub>3</sub> concentrations. Data in panels (a) to (d) are displayed as 1-  
 24 hour averages.

25

26

27

28



29

30 **Figure S3:** Panels (a) and (b) show the sensitivities of formic acid ions ( $\text{HCOO}^-$  at  $m/z$  45,  
 31  $\text{HCOO}\cdot\text{HF}$  at  $m/z$  65, and  $\text{SF}_4^-$  at  $m/z$  108) obtained from calibration measurements as a  
 32 function of ambient water vapor and  $\text{O}_3$  concentrations. Panels (c) and (d) show the acetic  
 33 acid sensitivity ( $\text{CH}_3\text{COO}\cdot\text{HF}$  at  $m/z$  79) obtained from calibration measurements as a  
 34 function of ambient water vapor and  $\text{O}_3$  concentrations.

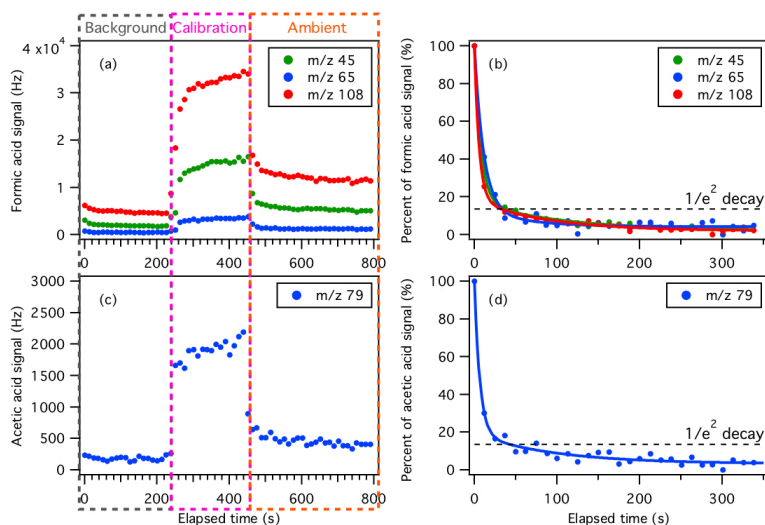
35

36

37

38

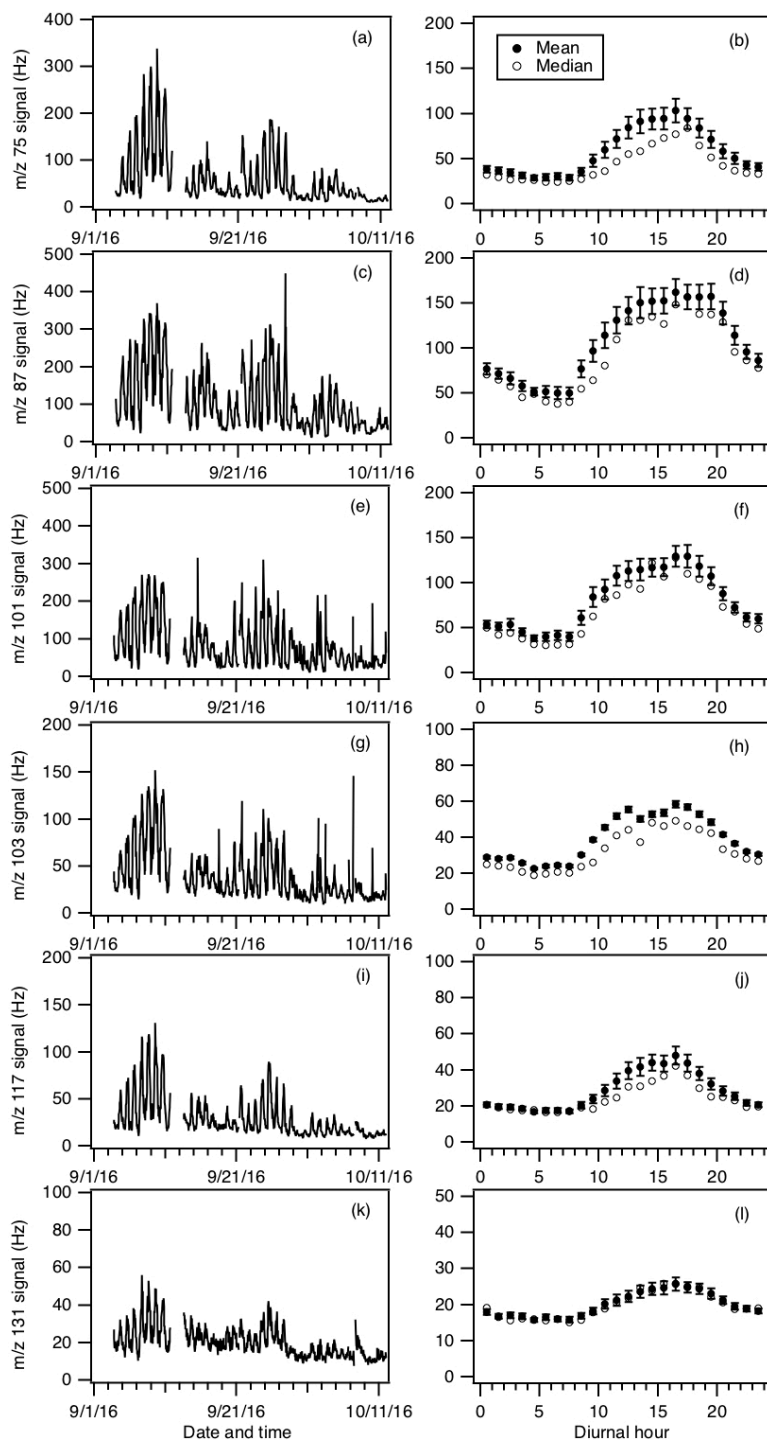
39



40

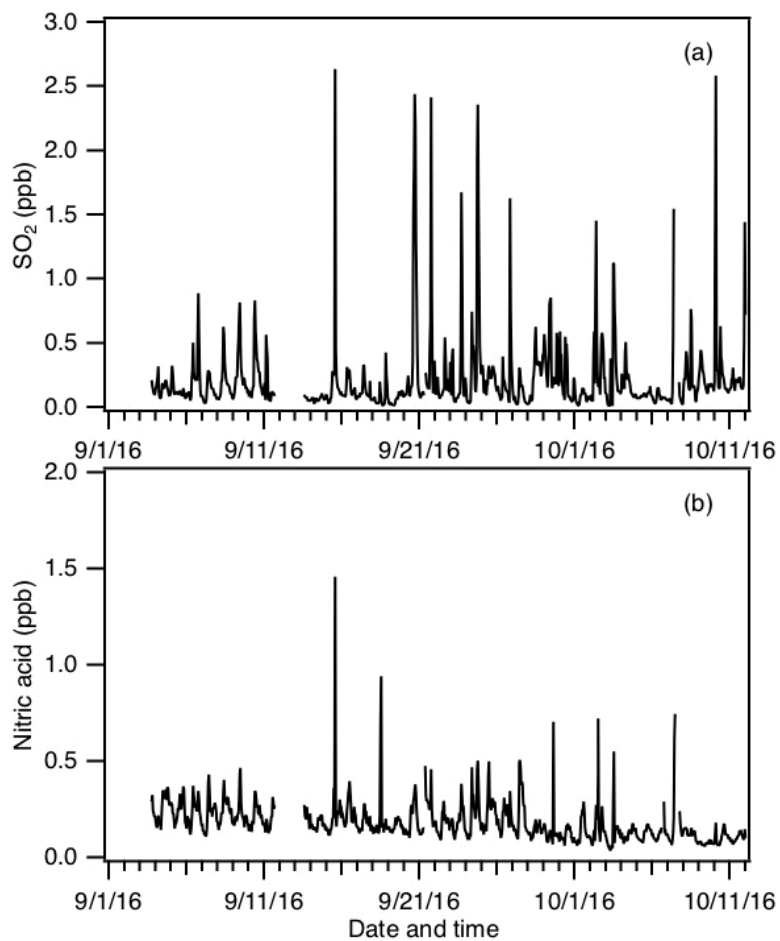
41 **Figure S4:** Example of the CIMS instrument response during switches between  
 42 background, calibration and ambient measurements of (a) formic, and (c) acetic acids.  
 43 Panels (b) and (d) show the percent of formic and acetic acid ion signals after the removal  
 44 of a 6.75 ppb of formic acid and 5.87 ppb of acetic acid standard addition calibration as a  
 45 function of time. The data shown here is 13 s time resolution data. Double exponential fits  
 46 to each m/z ion are shown as colored solid lines. Black dashed lines show the times for the  
 47 ions to decay to  $1/e^2$ .

48



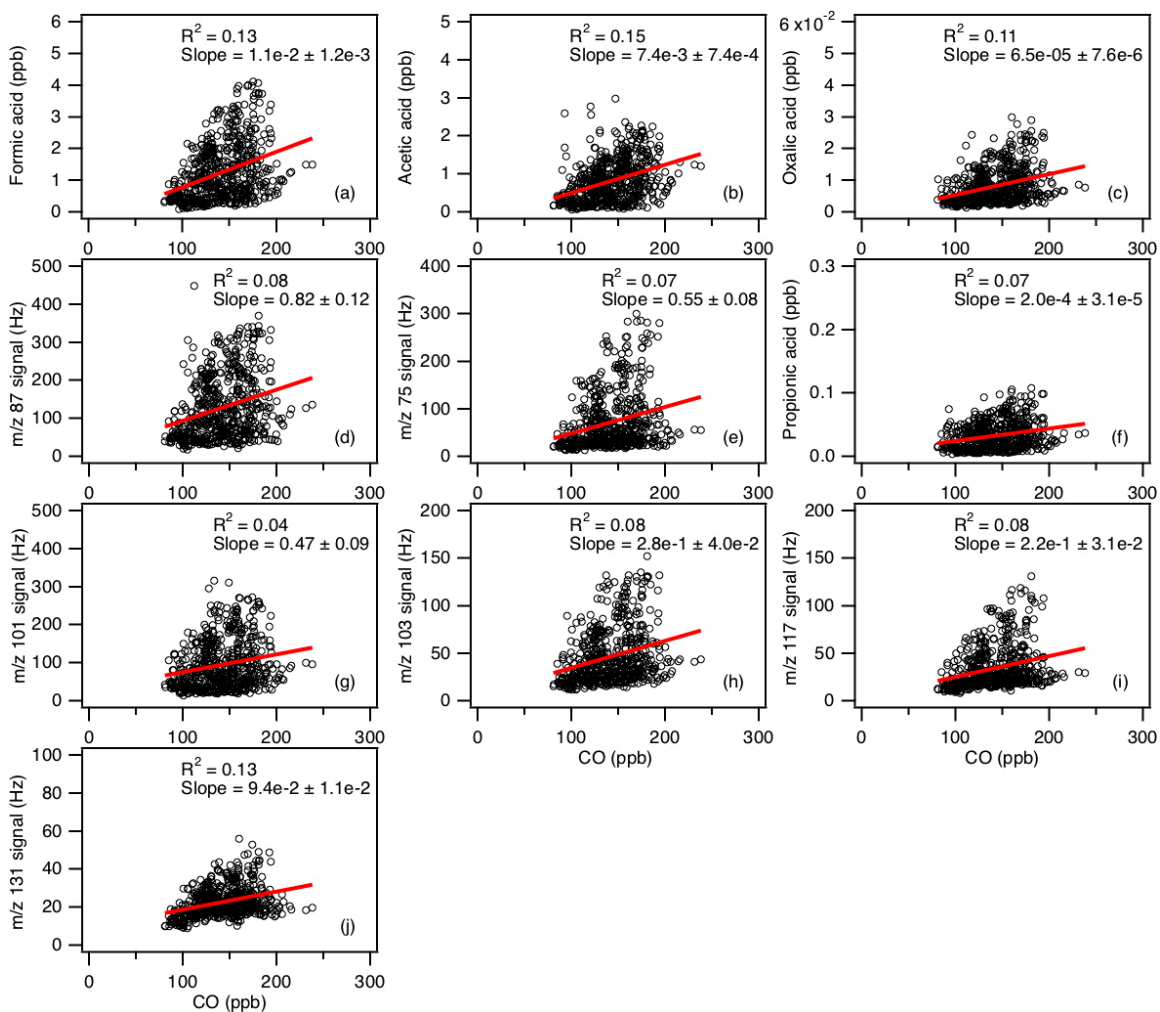
49

50 **Figure S5:** Time series and diurnal profiles of ion signals of organic acids with  $m/z$  75, 87,  
 51 101, 103, 117 and 131 measured during the field study. The data are displayed as 1-hour  
 52 averages. All the signals represent averages in 1-hour intervals and the standard errors are  
 53 plotted as error bars.



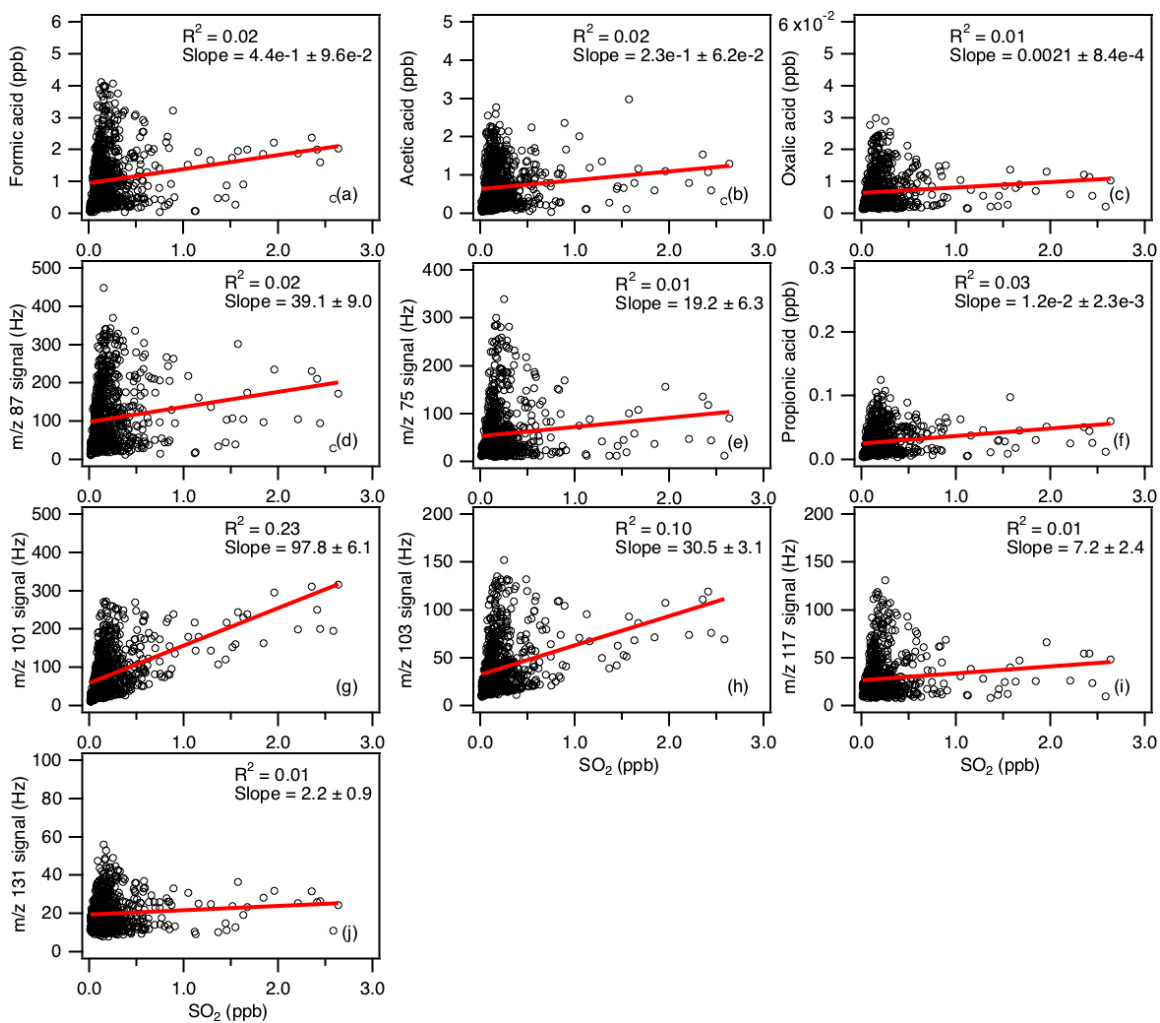
54

55 **Figure S6:** Time series of (a) SO<sub>2</sub> and (b) HNO<sub>3</sub> concentrations measured during the field  
56 study. All the data are displayed as 1-hour averages.



57

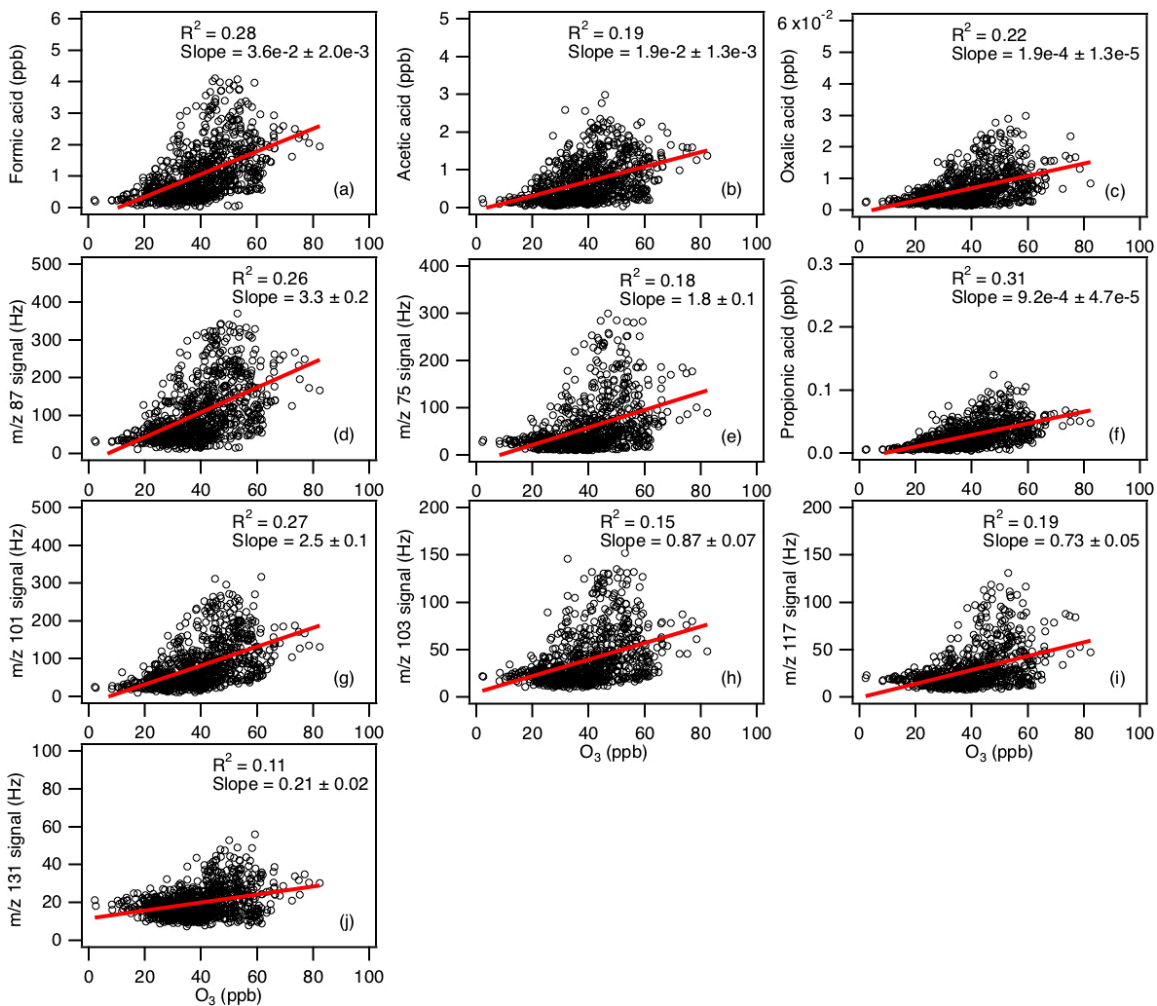
58 **Figure S7:** Scatter plots of concentrations (or ion signals) of the measured organic acids  
 59 with CO concentration. All the data are displayed as 1-hour averages. Red lines shown are  
 60 linear fits to the data.



61

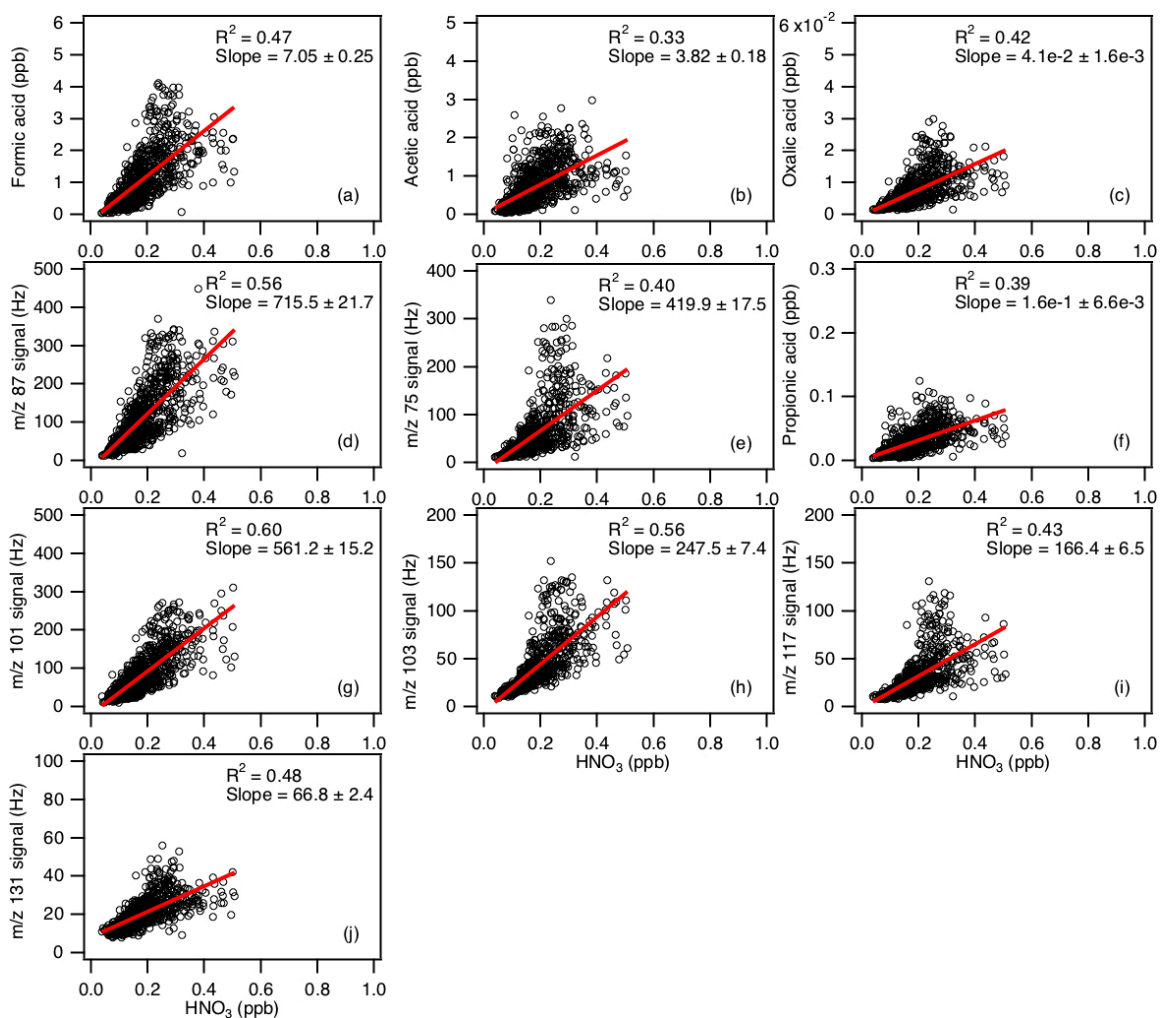
62 **Figure S8:** Scatter plots of concentrations (or ion signals) of the measured organic acids  
 63 with  $\text{SO}_2$  concentration. All the data are displayed as 1-hour averages. Red lines shown are  
 64 linear fits to the data.





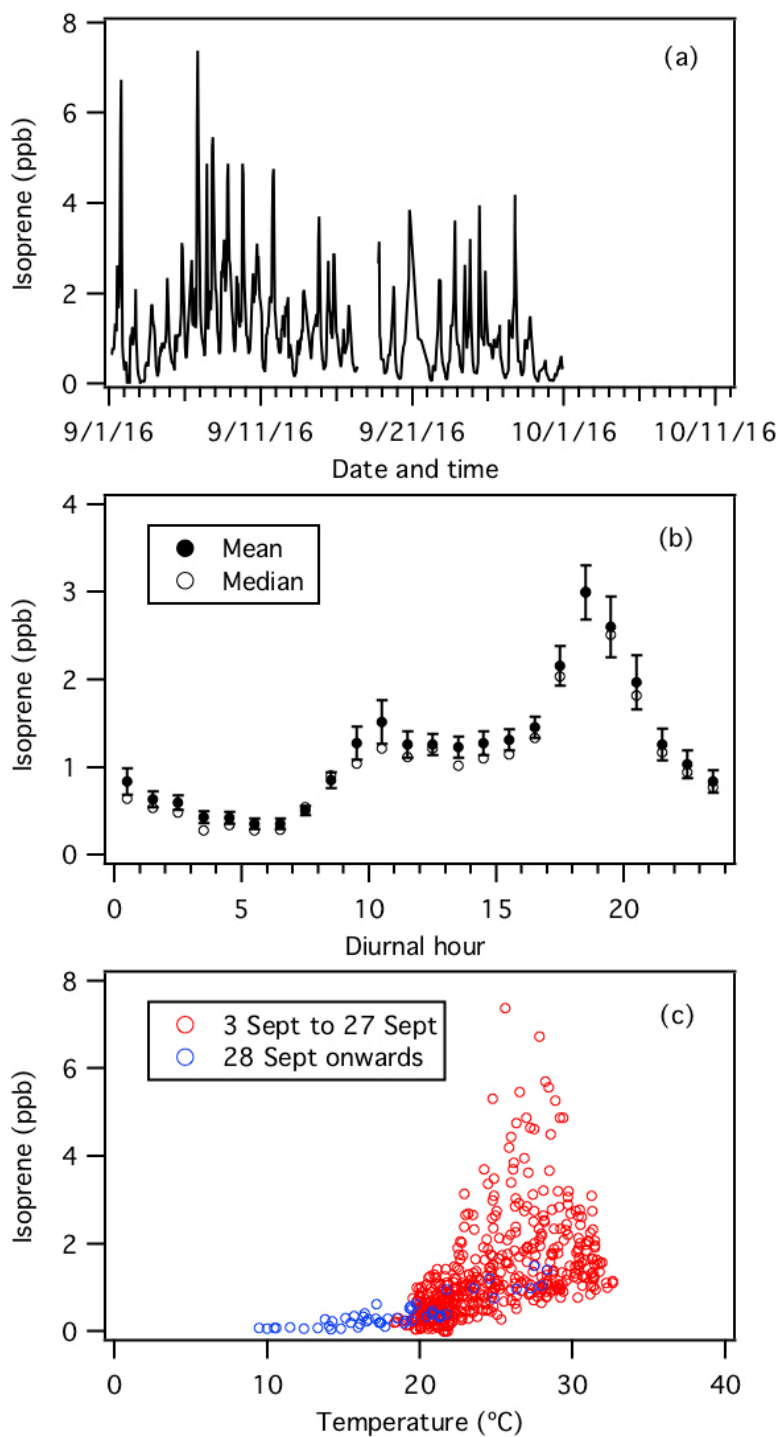
65

66 **Figure S9:** Scatter plots of concentrations (or ion signals) of the measured organic acids  
 67 with O<sub>3</sub> concentration. All the data are displayed as 1-hour averages. Red lines shown are  
 68 linear fits to the data.



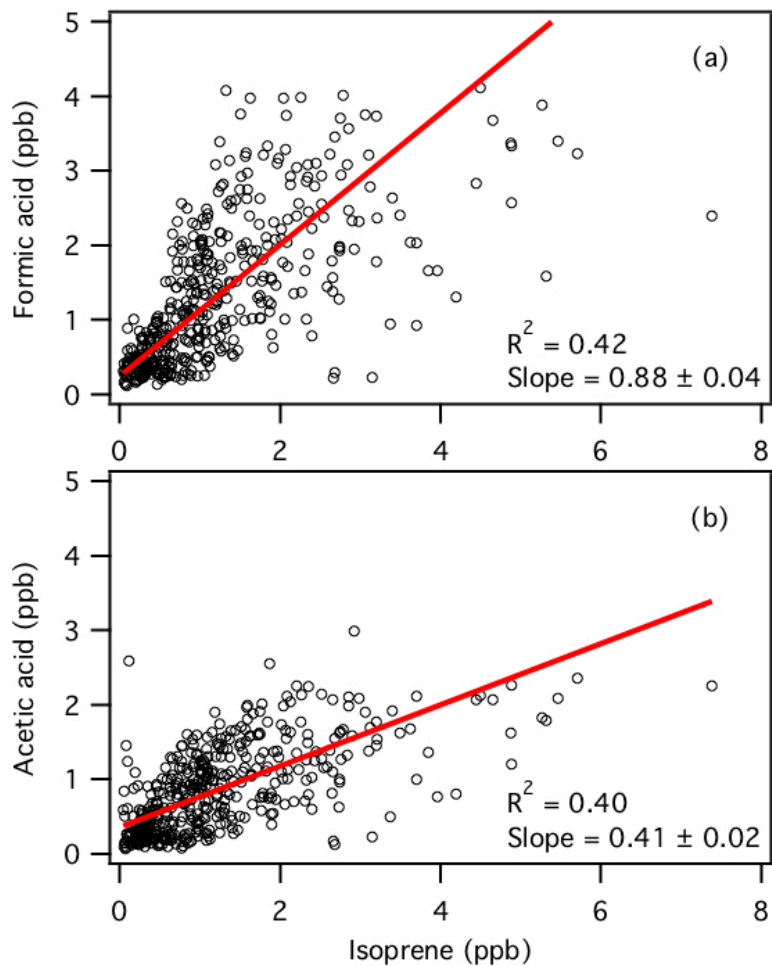
69

70 **Figure S10:** Scatter plots of concentrations (or ion signals) of the measured organic acids  
 71 with  $\text{HNO}_3$  concentration. To exclude periods when the site was affected by urban or power  
 72 plant emissions, data where  $\text{HNO}_3 > 0.5$  ppb are excluded from these scatter plots. All the  
 73 data are displayed as 1-hour averages. Red lines shown are linear fits to the data.



74

75 **Figure S11:** (a) Time series of isoprene concentration during the field study. (b) Diurnal  
 76 profile of isoprene. All the concentrations represent averages in 1-hour intervals and the  
 77 standard errors are plotted as error bars. (c) Scatter plot of isoprene concentration with  
 78 ambient temperature. All the data are displayed as 1-hour averages.



79

80 **Figure S12:** Scatter plots of concentrations of (a) formic and (b) acetic acids with isoprene  
81 concentration. All the data are displayed as 1-hour averages. Red lines shown are linear  
82 fits to the data.

83

84

85

86

87

88

89

90

91

92

93 Table S1a: Comparison of SF<sub>6</sub><sup>-</sup> vs. I<sup>-</sup> sensitivities of organic acids

<u>Organic Acid</u>	<u>I<sup>-</sup> sensitivity (Hz ppt<sup>-1</sup>)<sup>a</sup></u>	<u>SF<sub>6</sub><sup>-</sup> sensitivity (Hz ppt<sup>-1</sup>)</u>	
		<u>X<sup>-</sup></u>	<u>X<sup>-</sup>•HF</u>
<u>Formic acid</u>	<u>2.9</u>	<u>1.29 ± 0.22</u>	<u>0.29 ± 0.05</u>
<u>Acetic acid</u>	<u>0.1</u>	<u>1.46 ± 0.29</u>	<u>0.30 ± 0.06</u>
<u>Oxalic acid</u>	<u>0.21</u>	<u>6.38 ± 0.32</u>	<u>0.97 ± 0.05</u>
<u>Butyric acid</u>	<u>Not available</u>	<u>0.41 ± 0.01</u>	<u>0.12 ± 0.004</u>
<u>Glycolic acid</u>	<u>1.1</u>	<u>5.53 ± 0.11</u>	<u>1.64 ± 0.03</u>
<u>Propionic acid</u>	<u>0.066</u>	<u>2.05 ± 0.02</u>	<u>1.26 ± 0.01</u>
<u>Valeric acid</u>	<u>Not available</u>	<u>0.76 ± 0.008</u>	<u>0.35 ± 0.004</u>

94 <sup>a</sup>The I<sup>-</sup> sensitivities shown here are those reported by Lee et al. (2014). The organic acids  
 95 were detected as cluster ions with iodide (I(X)<sup>-</sup>).  
 96

97 Table S1b: Comparison of SF<sub>6</sub><sup>-</sup> vs. I<sup>-</sup> sensitivities of inorganic compounds

<u>Inorganic compound</u>	<u>I<sup>-</sup> sensitivity (Hz ppt<sup>-1</sup>)<sup>b</sup></u>	<u>SF<sub>6</sub><sup>-</sup> sensitivity (Hz ppt<sup>-1</sup>)</u>
<u>SO<sub>2</sub></u>	<u>0.028</u>	<u>2.9</u>
<u>HNO<sub>3</sub></u>	<u>9.0</u>	<u>5.8 for NO<sub>3</sub><sup>-</sup>, 0.2 for NO<sub>3</sub><sup>-</sup>•HF<sup>c</sup></u>
<u>HCl</u>	<u>0.03</u>	<u>1.4<sup>d</sup></u>

98 <sup>b</sup>The I<sup>-</sup> sensitivities shown here are those reported by Lee et al. (2018).

99 <sup>c</sup>The high collision energy used in the CDC promoted the dissociation of NO<sub>3</sub><sup>-</sup>•HF ions,  
 100 causing the low sensitivity at NO<sub>3</sub><sup>-</sup>•HF.

101 <sup>d</sup>HCl was detected as SF<sub>5</sub>Cl<sup>-</sup>.  
 102

### 103 References

104 [Lee, B. H., Lopez-Hilfiker, F. D., Mohr, C., Kurten, T., Worsnop, D. R., and Thornton, J.](#)  
 105 [A.: An Iodide-Adduct High-Resolution Time-of-Flight Chemical-Ionization Mass](#)  
 106 [Spectrometer: Application to Atmospheric Inorganic and Organic Compounds,](#)  
 107 [Environmental Science & Technology, 48, 6309-6317, 10.1021/es500362a, 2014.](#)

108 [Lee, B. H., Lopez-Hilfiker, F. D., Veres, P. R., McDuffie, E. E., Fibiger, D. L., Sparks, T.](#)  
 109 [L., Ebben, C. J., Green, J. R., Schroder, J. C., Campuzano-Jost, P., Iyer, S., D'Ambro, E.](#)  
 110 [L., Schobesberger, S., Brown, S. S., Wooldridge, P. J., Cohen, R. C., Fiddler, M. N.,](#)  
 111 [Bililign, S., Jimenez, J. L., Kurtén, T., Weinheimer, A. J., Jaegle, L., and Thornton, J. A.:](#)  
 112 [Flight Deployment of a High-Resolution Time-of-Flight Chemical Ionization Mass](#)  
 113 [Spectrometer: Observations of Reactive Halogen and Nitrogen Oxide Species, Journal of](#)  
 114 [Geophysical Research: Atmospheres, 0, doi:10.1029/2017JD028082, 2018.](#)